https://doi.org/10.5194/acp-2021-273
Preprint. Discussion started: 8 April 2021

Atmospheric Chemistry and Physics Discussions

Variability of nitrogen oxide emission fluxes and lifetimes estimated from Sentinel-5P TROPOMI observations

Kezia Lange[1], Andreas Richter[1], and John P. Burrows[1]

[1]Institute of Environmental Physics, University of Bremen, Bremen, Germany

Correspondence: Kezia Lange (klange@iup.physik.uni-bremen.de)

Abstract. Satellite observations of the high-resolution instrument TROPOMI on Sentinel-5 Precursor can be used to observe nitrogen dioxide (NO_2) at city scales, to quantify short time variability of NOx emissions and lifetime on a seasonal and daily basis. In this study, two years of TROPOMI NO_2 data, having a spatial resolution of 3.5 km x 5.5 km, together with ECMWF ERA5 wind data have been analyzed. NOx lifetimes and emission fluxes are calculated for 45 different NOx sources comprising cities and power plants, distributed around the world. The retrieved emissions are lower than the bottom-up emission inventories from EDGAR v5.0 but are in good agreement with other TROPOMI based estimates. Separation into seasons shows a clear seasonal dependence of emissions with in general the highest emissions during winter, except for cities in hot dessert climates, where the opposite is found. The NOx lifetime shows a systematic latitudinal dependence with an increase in lifetime from two to eight hours with latitude but only a weak seasonal dependence. For most of the 45 sources, a clear weekly pattern of emissions is found with weekend-to-week day ratios of up to 0.5, but with a high variability for the different locations. During the Covid-19 lockdown period in 2020 strong reductions in the NOx emissions were observed for New Delhi, Buenos Aires and Madrid.

1 Introduction

Nitrogen oxides (NOx) play a key role in atmospheric chemistry, air quality and climate. In the atmosphere NOx is defined as the sum of nitrogen monoxide and nitrogen dioxide (NOx = NO + NO_2). It is emitted into the atmosphere by both natural processes and anthropogenic activity. Natural sources include lightning, microbial processes in soils and naturally occurring wildfires. The dominant source of NOx is fossil-fuel combustion by anthropogenic activity, from traffic, residential heating, cooking and the industry and energy sectors. These sources are concentrated in cities and urban areas. In addition, biomass burning and the use of fertilizers are also significant sources of NOx.

These sources predominantly release NO. NO_2 is released in smaller amounts but is rapidly produced in the atmosphere where NO reacts with ozone (O_3). During the day NO_2 is photolyzed, reforming NO and producing an oxygen atom O, which forms O_3 in a termolecular reaction.

$$NO + O_3 \rightarrow NO_2 + O_2 \quad \text{(R1)}$$

https://doi.org/10.5194/acp-2021-273
Preprint. Discussion started: 8 April 2021

Atmospheric Chemistry and Physics Discussions

$$NO_2 + h\nu \rightarrow NO + O \quad \text{(R2)}$$

$$O + O_2 + M \rightarrow O_3 + M \quad \text{(R3)}$$

Depending on the concentrations of NO, NO_2 and O_3 and the diurnal variation of the photolysis frequency J_{NO_2} the rate of reactions R1, R2 and R3, respectively k_{NO+O_3}, J_{NO_2} and k_{O+O_2+M}, are rapid enough, that the Leighton photo-stationary state L is established and concentrations of NO and NO_2 are coupled in the daytime atmosphere by reactions R1-R3:

$$L = \frac{[NO]}{[NO_2]} = \frac{J_{NO_2}}{k_{NO+O_3} \cdot O_3}. \quad (1)$$

In the troposphere NOx is a precursor of the health hazard and greenhouse gas O_3 but NO_2 is also an important toxic health hazard in its own right (Jacob, 1999; Molina and Molina, 2004; Seinfeld and Pandis, 2006; Stocker, 2014). Consequently, monitoring and understanding its behavior is of particular importance in cities and urban agglomerations, where high emissions from multiple sources are found in combination with high population density. As a result, a large part of the population is exposed to polluted air.

NOx is short-lived in the atmosphere with a lifetime of several hours in the boundary layer during daytime (Beirle et al., 2003; Stavrakou et al., 2008). This explains in part the high spatial and temporal variability observed for NO_2. Other factors leading to large concentration gradients in NO_2 are its close relation to anthropogenic activity, the in-homogeneous distribution of sources, and variations of meteorological parameters, such as wind speed, temperature and illumination, which impact on the atmospheric lifetime and dilution of NO_2.

Investigation of seasonal emission estimates enables the disentanglement of the NOx sources in a region and the identification of their individual contributions (Van Der A et al., 2008). For example, it was found that for Paris in winter residential heating, rather than traffic emissions dominate the sources of NOx. This is not well accounted for in current emission inventories, in which residential heating is underestimated during winter and overestimated during summer (Lorente et al., 2019). In contrast, a seasonal cycle with a maximum of NOx emissions in summer was found for Riyadh, which, while not being significant in a statistical sense, may be explained by higher power consumption in summer caused by the use of air conditioning (Beirle et al., 2011).

NOx emissions also change from day to day, as a result of the human behavior, especially between work and rest days. Such patterns are readily identified (Beirle et al., 2003). Lorente et al. (2019) investigated the day-to-day variability of NOx emissions in Paris for individual days of 2018 with TROPOMI satellite measurements. They found that the highest emissions occurred on cold weekdays and the lowest on warm weekend days. In Chicago a clear weekend effect with reduced NOx emissions of 30 % during weekends was found analyzing one season of TROPOMI measurements (Goldberg et al., 2019). A recent study by Stavrakou et al. (2020) investigated the weekly NO_2 cycle and its trends using the long-term satellite observations of OMI and one year of TROPOMI NO_2 column measurements. For 115 out of 274 cities, significant weekly cycles were found. A

https://doi.org/10.5194/acp-2021-273
Preprint. Discussion started: 8 April 2021


Atmospheric Chemistry and Physics Discussions

weakening trend over Europe and the US could be observed. The opposite behavior was found for regions with increasing emissions. This provides evidence that NOx emissions are changing. The decreases or respectively increases in the contribution of anthropogenic emissions to the observed NO_2 levels are thus revealed. These long-term investigations provide valuable insight, but need to be complemented by analysis of daily, seasonal and annual means. Such analyses account better for the high variability of NOx emissions, resulting from fossil fuel combustion, which are monitored and limited by environmental policy regulations. In addition, sudden changes in emission patterns are readily identified (Vrekoussis et al., 2013).

Beginning in early 2020, first China and subsequently the majority of states around the world took containment measures to limit the spread of Covid-19. These measures resulted in significant changes of human behavior with reductions in traffic density and industrial activity and consequently anthropogenic emissions. Temporally finer resolved emission estimates help to identify the different potential origins of such changes. This provides an approach and an opportunity to better quantify source contributions and to distinguish between different anthropogenic and natural sources of NOx. Several recent studies have analyzed satellite measurements of NO_2 columns, and report substantial decreases in the NO_2 tropospheric column over China (Liu et al., 2020; Bauwens et al., 2020), northern Italy, South Korea and the United States (Bauwens et al., 2020). However, these reductions in NO_2 tropospheric columns cannot be simply attributed to a decrease in NOx emissions resulting from the Covid-19 containment measures. This is because of the high variability of NO_2 columns, which results from the rate of production and rate of loss of NO_2 and its transport. The tropospheric column of NO_2 is influenced by behavioral patterns of anthropogenic activity, seasonality, and meteorology. For example, Goldberg et al. (2020) found that the meteorology led to lower NO_2 values in spring 2020, as compared to spring 2019 in North America. This complicates the interpretation of the changes in NOx derived from comparisons between two particular years or also a particular year and an average of previous years. Consequently, Goldberg et al. (2020) combined TROPOMI NO_2 column data with ERA5 analysis and a chemical transport model to account for meteorology to calculate normalized NO_2 changes and a better representation of Covid-19 related NOx emission changes in North America. They found that in spring 2020 compared to spring 2019 NO_2 decreased between 9.2 % and 43.4 % for the 20 cities analyzed, with a median of 21.6 %.

In addition to NOx emissions, NOx lifetimes can be investigated with satellite data (Leue et al., 2001; Beirle et al., 2003; Kunhikrishnan et al., 2004). The NOx lifetime in daylight depends on the rate of loss of NOx which is attributed primarily to the reaction of the hydroxyl radical (OH) with NO_2 to form HNO_3. Consequently, there is a nonlinear relationship between the tropospheric concentrations of OH and NOx, which again depends in a complex fashion on the NOx concentration (Valin et al., 2013; Stavrakou et al., 2008). Laughner and Cohen (2019) showed that NOx lifetime has changed significantly between 2005 and 2014 in 30 North American cities, changes being of the same order of magnitude as those in NOx emissions. Another important factor influencing NOx lifetime is the actinic radiation photolyzing NO_2, which varies diurnally and is modulated by the presence of clouds. Shorter lifetimes at smaller solar zenith angles in summer or at lower latitudes due to higher photolysis frequencies are expected (Stavrakou et al., 2020). Typical lifetimes of NOx are between two and eight hours in polluted air masses and extend to about a day for cleaner more rural background concentrations for which nighttime chemistry also has to be considered (Beirle et al., 2011; Valin et al., 2014; de Foy et al., 2014; Seinfeld and Pandis, 2006). Studies for winter months and especially for winter months at higher latitudes are limited, but analyses with GEOS-Chem show a tendency towards longer

https://doi.org/10.5194/acp-2021-273
Preprint. Discussion started: 8 April 2021


Atmospheric Chemistry and Physics Discussions

lifetimes of about one day (Martin et al., 2003; Shah et al., 2020).

Adequate spatially and temporally resolved measurements of NOx are required to assess and compare the variability of NOx emissions and lifetimes around the world. The different urban NOx sources include different types and patterns of emissions, mixtures of domestic and transport emissions, often mixed with industrial sources and sometimes also dominated by emissions from power plants of different types or even oil refineries, etc. Provided the tropospheric NO_2 columns retrieved from satellite sensors have sufficient spatial resolution, the typically short daytime lifetime of NOx in urban agglomerations provides an opportunity to disentangle and quantify the local sources of NOx and their variations over time.

The TROPOspheric Monitoring Instrument (TROPOMI) on Sentinel-5 Precursor (S5P), which was launched in October 2017, provides higher spatial resolution than its predecessors. Tropospheric columns of NO_2 retrieved from TROPOMI thus offer the best opportunity so far to deconvolve urban daytime sources of NOx (Veefkind et al., 2012; Griffin et al., 2019).

For the urban areas targeted, we assume that two years tropospheric NO_2 columns retrieved from TROPOMI provide a sufficient data set to be separated into the following time periods: Seasons, weekend and working days, and times before and during Covid 19 restrictions to examine short-term variability. In this study, we show that the spatial resolution and good signal-to-noise ratio of TROPOMI NO_2 columns allow to investigate NOx sources at city level, for isolated power plants and even for sources with low NOx emissions. We use the method first developed by Beirle et al. (2011) and refined by later studies (Pommier et al., 2013; Valin et al., 2013) to estimate the NOx emissions and lifetimes from TROPOMI NO_2 column amounts. Studies on NOx emissions and lifetimes have been reported for OMI data, which have coarser spatial resolution, for a limited number of sources and using longer time periods of data (Ialongo et al., 2014; de Foy et al., 2015; Lu et al., 2015; Liu et al., 2016). Other studies, which applied this method to TROPOMI data are reported by Goldberg et al. (2019) and Lorente et al. (2019). In this work, we provide the first study of NOx emissions and lifetimes for a large data set, comprising 45 different NOx source regions distributed over the world. Focus of our investigation is to assess the variability of NOx emissions and lifetimes in space and time during the period of observation.

2 Data

2.1 TROPOMI NO_2 tropospheric vertical column

In October 2017, the Copernicus Sentinel-5 Precursor (S5P) satellite with the TROPospheric Monitoring Instrument TROPOMI) on board was launched into a sun-synchronous orbit at 824 km altitude. TROPOMI comprises a hyperspectral spectrometer measuring radiation in the ultraviolet (270 nm - 320 nm), visible (310 nm - 500 nm) and infrared (675 nm - 775 nm, 2305 nm - 2385 nm) spectral regions (Veefkind et al., 2012). The two-dimensional CCD detectors measure spectra in 450 separate viewing directions across the 2600 km swath with an integration time of approximately one second. This results in a high spatial resolution of 3.5 km x 7 km in nadir with little variation across the swath. In August 2019, the pixel size was reduced further to 3.5 km x 5.5 km by reducing along track averaging. One orbit around the Earth takes about 100 minutes, which, in combination with the wide swath, results in a daily global coverage. At higher latitudes, two to three useful overpasses are available on the

https://doi.org/10.5194/acp-2021-273
Preprint. Discussion started: 8 April 2021


Atmospheric Chemistry and Physics Discussions

same day with approximately 100 minutes in between the measurements. The equator overpass time of S5P is 13:30 Mean Local Solar time in the ascending node.

The different spectral ranges of TROPOMI provide information about the atmospheric abundance of various trace gases including the operational products: O_3, methane (CH_4), carbon monoxide (CO), sulfur dioxide (SO_2), formaldehyde (HCHO), clouds, aerosol layer height, aerosol index and NO_2. In addition, there are valuable non-operational products such as glyoxal (CHO.CHO) (Alvarado et al., 2020) or bromine monoxide (BrO) (Seo et al., 2019). In this study, the operational NO_2 product of TROPOMI is used (Van Geffen et al., 2018). The NO_2 product from TROPOMI extends NO_2 measurements from earlier instruments such as GOME (1995-2011, (Burrows et al., 1999)), SCIAMACHY (2002–2012, (Bovensmann et al., 1999)), GOME-2 (since 2007, (Munro et al., 2006)), OMI (since 2004, (Levelt et al., 2006)) and OMPS (since 2011, (Dittman et al., 2002)). These instruments had increasing spatial coverage and resolution, OMI being the first instrument with daily global coverage. However, with a resolution of $13\,\mathrm{km}$ x $24\,\mathrm{km}$ at nadir, its spatial resolution is one order of magnitude poorer than that of TROPOMI in the center of the swath and much lower at the edges.

The level-1b spectra measured by TROPOMI are analyzed with the Differential Optical Absorption Spectroscopy (DOAS) technique in the fitting window $405\,\mathrm{nm}$ - $465\,\mathrm{nm}$. The retrieved NO_2 slant column densities are separated into a stratospheric and a tropospheric part based on data assimilation by the TM5-MP global chemistry transport model. The resulting tropospheric slant columns are then converted to tropospheric vertical columns by tropospheric air mass factors (AMFs) based on a look-up table of altitude-dependent AMFs, NO_2 vertical profiles from the TM5-MP model, the OMI climatological surface albedo and cloud characteristics derived using the FRESCO algorithm (Van Geffen et al., 2018). The final product is the tropospheric vertical column, defined as the vertically integrated number of molecules per unit area between the surface and the tropopause.

In this study, we use the operational level-2 TROPOMI tropospheric vertical column NO_2 product from March 2018 to November 2020. This includes the reprocessed (RPRO) and offline mode (OFFL) data of version V01.00.01 to version V01.03.02. Due to changes with version V01.04. from 29 November 2020, we only use the data up to 28 November 2020 for our analysis to ensure better comparability. Data from 30 April 2018 onwards is freely available on https://s5phub.copernicus.eu/. The data with a spatial resolution of up to $3.5\,\mathrm{km}$ x $5.5\,\mathrm{km}$ are oversampled to a finer resolution of $0.01°$ x $0.01°$. Each TROPOMI ground pixel is accompanied by a quality assurance value (qa_value). The qa_value ranges from zero (error, no output) to one (no errors or warnings) and indicates the quality of the processing and retrieval result. Based on the recommendation by Van Geffen et al. (2018), measurements with a qa_value lower than 0.75 are filtered and not used. A qa_value of 0.75 removes part of the scenes covered by snow and ice, problematic retrievals and also excludes measurements with cloud radiance fractions of more than $50\,\%$, which roughly corresponds to a geometric cloud fraction of 0.2.

Figure 1 shows the average NO_2 tropospheric vertical column from May 2018 to December 2019. The red circles mark regions with higher NO_2 than their surroundings and are analyzed in this study.

https://doi.org/10.5194/acp-2021-273
Preprint. Discussion started: 8 April 2021

Atmospheric Chemistry and Physics Discussions

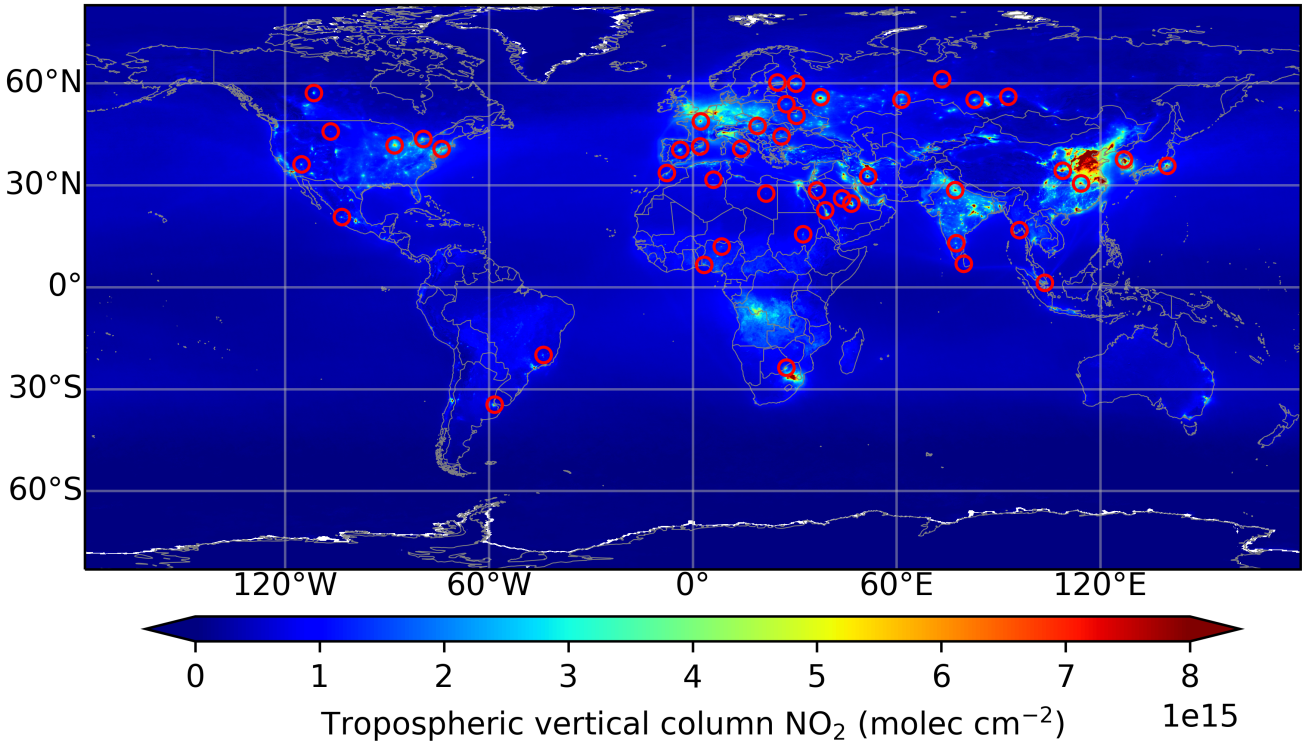

Figure 1. NO_2 tropospheric vertical column of the offline, level-2 Sentinel-5P TROPOMI product from 04 May 2018 to 31 December 2019. Red circles mark NOx emission sources analyzed in this study.

2.2 Wind data

In addition to the TROPOMI NO_2 data, wind speed and direction are required for the emission and lifetime calculations. The wind data used are provided by the European Centre for Medium-Range Weather Forecast (ECMWF), ERA5 reanalysis hourly data with a horizontal resolution of 0.25° x 0.25°. To merge the wind data in space and time with the TROPOMI observations, they are interpolated to the overpass time and oversampled to the same 0.01° x 0.01° resolution as the TROPOMI data. Beirle et al. (2011) investigated the dependence of calculated emissions and lifetimes on the wind data level height by comparing the results calculated with wind fields averaged from ground up to 500 m, 200 m and 1000 m and showed low dependence of the results on the wind level height. We use the wind data from the 100 m level above ground. In urban areas, NOx is predominantly emitted near the surface, while power plants emit into higher atmospheric layers depending on stack height. At the early afternoon overpass of TROPOMI, it can be assumed that the boundary layer is well mixed and the 100 m level is representative for the emissions investigated in this study.

https://doi.org/10.5194/acp-2021-273
Preprint. Discussion started: 8 April 2021


Atmospheric Chemistry and Physics Discussions

2.3 Ozone mixing ratios

Ozone mass mixing ratios, for scaling the NO_2 column measurements to NOx columns to estimate emissions in terms of NOx, were taken from the Copernicus Atmosphere Monitoring Service (CAMS) reanalysis EAC4. The latter is the latest ECMWF global reanalysis of atmospheric composition. The CAMS reanalysis combines observations with model data into a globally complete and consistent data set. It is gridded with a 0.75° x 0.75° horizontal resolution and has a monthly temporal resolution with three hourly estimates. The vertical resolution consists of 60 model levels, with the top level at 0.1 hPa (Inness et al., 2019). We used the monthly averages for 2019 at 950 hPa, interpolated to a typical mean early afternoon S5P overpass time. Conversion from ozone mass mixing ratios mr_{O_3} ($kg\,kg^{-1}$) to ozone number density n_{O_3} is performed using:

$$n_{O_3} = mr_{O_3} \cdot \frac{m_w}{m_{O_3}} \cdot M \tag{2}$$

with atmospheric number concentration M:

$$M = \frac{p}{k_b \cdot T}. \tag{3}$$

Using pressure p = 950 hPa and Temperature T at 950 hPa from the CAMS reanalysis, Boltzmann constant k_b, molar mass of ozone m_{O_3} and molar mass of humid air m_w calculated with specific humidity at 950 hPa from the CAMS reanalysis.

2.4 Emission inventories

For comparison with the calculated TROPOMI NOx emissions, we use the bottom-up emission inventory EDGAR v5.0 of 2015. The emission data are available in 0.1° x 0.1° gridded resolution. For calculation of total emissions in the specific source regions, the gridded emission inventory data have to be integrated over the area for which the top-down method based on TROPOMI data is sensitive. The EDGAR inventory is based on activity data (i.e. population, energy, fossil fuel production, industrial processes, agricultural statistics), mainly from the International Energy Agency (IEA), corresponding emission factors, national and regional information on technology mix data and end-of-pipe measures (Crippa et al., 2018, 2019). Uncertainties in bottom-up inventories are inferred from the dependence of emission factors on the fuel type, technology and combustion condition, as well as the low-resolution activity data and emission factors. The uncertainty in NOx emissions from the latest EDGAR inventory version (v4.3.2) varies from 17 % to 69 % for different regions (Crippa et al., 2018). The limited temporal coverage of bottom-up emissions results in additional uncertainties. 2015 is the most recent year available in EDGAR v5.0, which cannot reflect recent declines in NOx emissions or new sources of NOx, which were found in trend analysis of NO_2 column satellite data (Georgoulias et al., 2019). Thus, we anticipate for the majority of analyzed regions that the TROPOMI estimates are lower than the EDGAR inventory estimates for 2015.

3 Method

The method to estimate emissions and lifetimes from satellite column data builds on the heritage of the method introduced by Beirle et al. (2011) and refined by later studies (Pommier et al., 2013; Valin et al., 2013). We use two years of TROPOMI NO_2

https://doi.org/10.5194/acp-2021-273
Preprint. Discussion started: 8 April 2021

Atmospheric Chemistry and Physics Discussions

tropospheric vertical column data from 01 March 2018 to 29 February 2020 for the general analysis and the months January through November of 2019 and 2020 for the Covid-19 impact study in section 4.5. The three steps of the analysis are shown in Fig. 2 for the Medupi and Matimba power plants in South Africa as an example. First, the source region is selected. The choice of sources is described in more detail in section 3.1. The next step is a rotation of the satellite measurements around the selected source with the corresponding ERA5 reanalysis wind data to a common wind direction resulting in an upwind-downwind pattern, which is described in more detail in section 3.2. The NO_2 column of each pixel is converted into NOx column and the mean NOx distribution is calculated. In the last step, we apply a line density fit with an exponentially modified Gaussian (EMG) function to the averaged NOx columns to calculate the NOx emission and lifetime (see section 3.3).

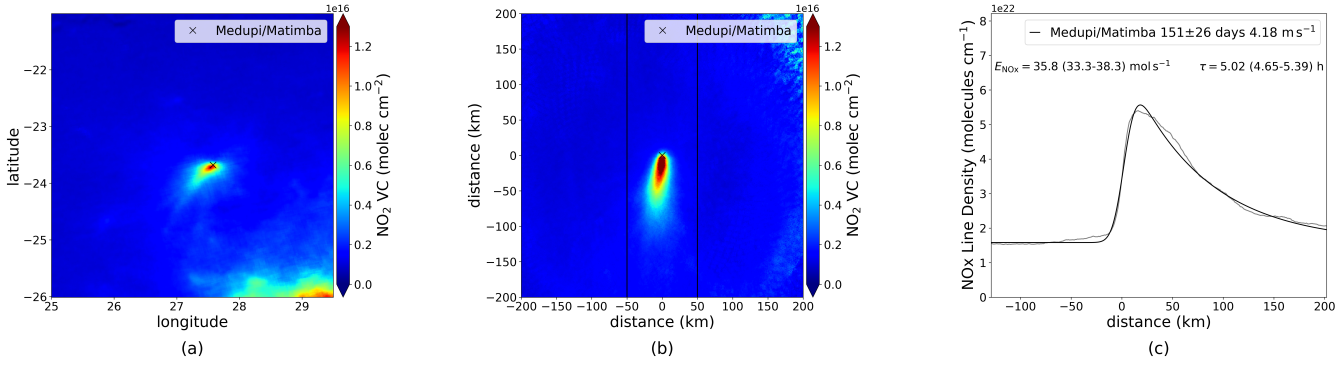

Figure 2. (a) Mean NO_2 tropospheric vertical column from 01 March 2018 to 29 February 2020 in the region of the power plants Medupi and Matimba in South Africa for days with wind speed > $2\,\mathrm{m\,s^{-1}}$. (b) Each TROPOMI pixel of the two-year time period rotated with its wind direction around the source (cross) to an upwind-downwind pattern. Black lines indicate a sector of $\pm 50\,\mathrm{km}$ around the source. (c) NOx line density as function of distance to the source calculated for the $\pm 50\,\mathrm{km}$ sector (gray) and fit results (black) with estimated emission and lifetime. Emission and lifetime uncertainties are 1-sigma uncertainties derived by the fitting procedure.

3.1 Selection of sources

To obtain a representative analysis of the variability of NOx emissions and lifetimes from urban and industrial areas around the earth, we have used the following guideline for the selection of targets. The targeted emission sources need to be well distributed around the world to provide information about the seasonal variations, climatic conditions, latitudinal dependence and weekday behavior of the NOx lifetimes and emissions. By visually inspecting the global mean NO_2 tropospheric vertical column distribution, we selected 45 target regions for the calculation of emissions and lifetimes. The selected sources comprise a mix of cities with predominantly domestic and transport emissions e.g. Paris (France), cities with more industrial emitters e.g. Chelyabinsk (Russia), power plants like Medupi and Matimba in South Africa or oil refinery regions like Sarir Field in Libya. The method works best for isolated point sources with a high contrast between source and background. Regions having low cloud coverage are preferred to maximize the number of satellite observations. In addition, a local meteorology for the target region, having rather homogeneous wind patterns, facilities the detection of the outflow patterns (Beirle et al., 2011). Some,

https://doi.org/10.5194/acp-2021-273
Preprint. Discussion started: 8 April 2021


Atmospheric Chemistry and Physics Discussions

initially promising sources like Santiago de Chile, were omitted. This was a result of their location in coastal and mountainous regions with inhomogeneous terrain. This results in inhomogeneous wind patterns, which are more difficult to interpret and leads to larger uncertainties in NOx emission rates and lifetimes.

For this study, many of the sources with high NO_2 signal in China were not used, because the influence of large NOx emitting sources nearby resulted in low contrast of the NO_2 column amount between the target and the local background. For such conditions, other methods to determine NOx emission rates and lifetimes are more appropriate (Liu et al., 2016). Not every source region is used for every analysis in this study because of data availability after separating data into seasons or week and weekend days. Due to the high spatial resolution and the good signal to noise ratio of the TROPOMI data, it is possible to use a data set of only two-years length to analyze successfully regions, which are covered more frequently by clouds or have low NO_2 signals. From the 45 targeted regions, three are in the southern hemisphere. In order to integrate them into the analysis, they are mirrored in latitude and shifted by six months in season. All source regions are listed in the appendix table A1. Surgut (Russia) is the NOx source with the highest latitude at 61.25° N, and Singapore (Singapore) is closest to the equator at 1.3° N. Figure 2 (a) shows the average of NO_2 tropospheric vertical columns for two years of data from 1 March 2018 to 29 February 2020 for days with wind speeds > $2\,\mathrm{m\,s^{-1}}$ in the region of the power plants Medupi and Matimba in South Africa. This is an example for one of the selected source regions. The NO_2 distribution shows an isolated source and its plume which has a high contrast to a low background concentration. In the south eastern part of the map high tropospheric NO_2 columns are visible. These originate from the South African Highveld conurbation near Johannesburg.

3.2 Rotation technique

To investigate the spatial pattern of NO_2 column measurements we combine the approach from Beirle et al. (2011) of a directional classification to determine the distribution, as a function of downwind distance, with a rotation of each TROPOMI measurement with its merged wind direction around the source to a common wind direction (Pommier et al., 2013; Valin et al., 2013).

Each TROPOMI observation is merged with the ERA5 wind data and rotated with its wind direction about a reference point (e.g. the city centre or the power plant site) to a common wind direction, preventing a neutralization of outflow patterns of opposite wind directions. After the rotation, the TROPOMI measurement points are redistributed along the upwind-downwind direction with the enhancement located in the downwind area of the source reference point and a clear outflow pattern. The measurement points maintain their upwind-downwind character and are analyzed simultaneously, independent of their wind direction. Figure 2 (b) shows the mean of the rotated NO_2 tropospheric vertical column for the Medupi/Matimba example, where a pronounced plume with a clear upwind-downwind distribution is found. The black lines indicate a sector of $\pm\,50\,\mathrm{km}$ around the source. Only data in this sector are used in the next step for the calculation of emission and lifetime. As an additional quality filter, only days, where $50\,\%$ of the ground scenes in this area contain measurements and are not filtered because of clouds or wind speed, are used in the analysis.

https://doi.org/10.5194/acp-2021-273
Preprint. Discussion started: 8 April 2021


Atmospheric Chemistry and Physics Discussions

3.3 Line density calculation

The average outflow pattern of the NO_2 tropospheric vertical column with a decay of the signal with distance from the reference source point reflects transport and nonlinear effects of atmospheric chemistry. Beirle et al. (2011) proposed a model to estimate the NOx emissions and lifetimes by integrating the mean NO_2 columns in the across-wind direction and thereby reducing the two-dimensional maps to one-dimensional so-called line densities with units molecules cm^{-1}. In this study, we first converted the NO_2 columns for each pixel into NOx columns to obtain NOx line densities from which NOx emissions are calculated directly (comparable to Beirle et al. (2021)) instead of applying the commonly used fixed [NOx]/[NO_2] ratio of 1.32. Assuming that the Leighton photostationary state applies for the polluted air masses investigated, the NO_2 is considered a surrogate for NOx and concentrations of NO and NO_2 are coupled by:

$$\frac{[\mathrm{NOx}]}{[\mathrm{NO_2}]} = 1 + \frac{[\mathrm{NO}]}{[\mathrm{NO_2}]} = 1 + \frac{J_{\mathrm{NO_2}}}{k_{\mathrm{NO+O_3}} \cdot n_{\mathrm{O_3}}} \tag{4}$$

with $J_{\mathrm{NO_2}}$ the photolysis frequency of NO_2 and $k_{\mathrm{NO+O_3}}$ the rate constant for the reaction of NO with O_3.

The O_3 mixing ratios are taken from the CAMS reanalysis data set converted to number densities $n_{\mathrm{O_3}}$ and interpolated to a typical mean early afternoon S5P overpass time as described in section 2.3.

For clear-sky conditions the photolysis frequency in the boundary layer is parameterized as a function of solar zenith angle (SZA) as proposed by Dickerson et al. (1982):

$$J_{\mathrm{NO_2}} = 0.0167 \exp\left(-\frac{0.575}{\cos(\mathrm{SZA})}\right) s^{-1}. \tag{5}$$

The rate constant $k_{\mathrm{NO+O_3}}$ can in general be well represented by the Arrhenius expression, following the recommendation by Atkinson et al. (2004):

$$k_{\mathrm{NO+O_3}}(T) = 2.07 \cdot 10^{-12} \exp\left(-\frac{1400}{T}\right) \tag{6}$$

with temperature T taken from the monthly mean values in hourly resolution from the CAMS reanalysis data set interpolated to the mean S5P overpass time.

From the averaged NOx columns NOx line densities are calculated by integrating perpendicular to the wind direction. To reduce the influence of possible surrounding sources, the line density is only calculated in a sector around the source (black vertical lines in Fig. 2 (b)), which does not cut the plume and thereby miss emissions. Typical values used for the sector size are between $\pm 15\,\mathrm{km}$ and $\pm 70\,\mathrm{km}$ across the plume depending on its width, and up to $200\,\mathrm{km}$ upwind and up to $400\,\mathrm{km}$ downwind of the source depending on plume length and the presence of other influencing sources. Figure 2 (c) shows the calculated line density as function of distance to the source. The calculated line density is shown in gray and the fit in black. Due to transport processes, the maximum is shifted in wind direction and the line density curve is steep upwind and less steep downwind with an exponential decay. From this line density curve, NOx lifetime and emission can be estimated. The fitting model M as function of distance to the source x is described by (similar to Beirle et al. (2011) supplement):

$$M(x) = E' \cdot (e \otimes G)(x) + B \tag{7}$$

https://doi.org/10.5194/acp-2021-273
Preprint. Discussion started: 8 April 2021

Atmospheric Chemistry and Physics Discussions

with a convolution of the exponential e and the Gaussian G function scaled by a multiplicative emission factor E' and a background concentration offset B. The exponential function describes transport and chemical decay:

$$e(x) = \exp\left(\frac{-(x-X)}{x_0}\right) \tag{8}$$

with $x > X$ (downwind) and else zero, where X is the location of the apparent source relative to the source reference point and x_0 the distance over which the line density decreases by a factor of e (e-folding distance). The Gaussian function represents the broadening of the source by spatial smoothing with the Gaussian function width σ, which accounts for spatial smoothing caused by the extent of the spatial source, the TROPOMI pixel size and wind variations:

$$G(x) = \frac{1}{\sqrt{2\pi}\sigma}\exp\left(-\frac{x^2}{2\sigma^2}\right). \tag{9}$$

This results in:

$$\begin{aligned} M(x) &= E' \cdot \left(\exp\left(\frac{-(x-X)}{x_0}\right) \otimes \frac{1}{\sqrt{2\pi}\cdot\sigma}\cdot\exp\left(-\frac{x^2}{2\cdot\sigma^2}\right)\right) + B \\ &= \frac{E'}{2}\cdot\exp\left(\frac{\sigma^2}{2\cdot x_0^2} - \frac{x-X}{x_0}\right)\cdot\operatorname{erfc}\left(\frac{\sigma^2 - x_0(x-X)}{\sqrt{2}\cdot\sigma\cdot x_0}\right) + B. \end{aligned} \tag{10}$$

The fitted e-folding distance x_0 and the mean wind speed w from the line density sector was then used to calculate the mean lifetime:

$$\tau = \frac{x_0}{w}. \tag{11}$$

The calculated lifetime includes effects of deposition, chemical conversion and wind advection but must be considered as an effective mean dispersion lifetime. This is because, downwind changes for example due to a changing [NO_2]/[NOx] ratio in the plume are not considered in the method used.

The multiplicative emission factor E' characterizes the total amount of NOx near the source and is used together with the mean wind speed w from the line density sector to derive the NOx flux in $\mathrm{mol\,s^{-1}}$:

$$E_{\mathrm{NO_2}} = \frac{E'}{N_\mathrm{A}}\cdot w \tag{12}$$

with the Avogadro's constant $\mathrm{N_A} = 6.02214076\cdot 10^{23}\,\mathrm{mol^{-1}}$.

The described method to calculate emissions and lifetime will be named exponentially modified Gaussian (EMG) method. Uncertainties and error bars for emission and lifetime estimates are based on 1-sigma uncertainties (standard deviation) derived by the EMG fitting procedure and are calculated with error propagation. Uncertainties in general are discussed in more detail in section 4.6.

4 Results and Discussion

The EMG method was applied to the mean TROPOMI NO_2 column data of the selected regions and NOx emissions and lifetimes were calculated. For all available TROPOMI measurements of the two years period from 01 March 2018 to 29 February

https://doi.org/10.5194/acp-2021-273
Preprint. Discussion started: 8 April 2021


Atmospheric Chemistry and Physics Discussions

2020, and also separated into seasons, working days and weekends and pre Covid-19 times and the Covid-19 pandemic. Not all source regions are used for all analysis due to sometimes poor statistics when separating the two years of data into specific periods.

4.1 Comparison to EDGAR emission data base and other studies

The retrieved NOx emissions for the two years of data are compared to the EDGAR emission data base. Figure 3 shows a scatter plot of the resulting NOx emissions for the 45 source regions versus the respective emissions received from the EDGAR data base for the year 2015. Most NOx source regions have higher emissions in the EDGAR database than estimated by the EMG method in this study. One possible explanation for differences is the different time periods the two methods are based on with 2015 for the EDGAR database and March 2018 to February 2020 for this study. In addition, the EMG method is only sensitive to daytime emissions on nearly cloudless days close to the time of measurements, whereas the EDGAR data base gives 24-hour annual averages. Another possible explanation is the known low bias of current TROPOMI tropospheric NO_2 columns, as compared to ground based or aircraft measurements of the tropospheric NO_2 column. This underestimation is more pronounced for regions with larger NO_2 columns (Verhoelst et al., 2021), which is in agreement with our finding that differences to EDGAR are largest for the source regions with high emissions such as Riyadh, Singapore, Seoul, New York and Tokyo. This underestimation of TROPOMI is discussed in more detail in section 4.6. The calculated emissions for the Medupi and Matimba power plants are an exception as they show significantly higher emissions estimated by the EMG method than reported in the EDGAR data base. One likely explanation for this observation is that the Medupi power plant was put in operation only in 2015, the year to which the EDGAR data base refers to. Consequently, it was not or only partially considered in EDGAR.

The NOx emission estimates from this study are also compared to results from other recent studies (Beirle et al., 2019; Goldberg et al., 2019; Lorente et al., 2019), which estimated NOx emissions with TROPOMI data. The studies used for comparison focused only on specific regions, used different periods, and the methods differ slightly but have in common that all used TROPOMI data for their emission calculations. Table 1 compares the NOx emission estimates for all source regions used in the comparative studies to the emission estimates retrieved in this study. Due to different time periods and slightly different methods, differences are expected but in general the emissions are in good agreement. Beirle et al. (2019) used modified operational NO_2 data, for the period from December 2017 to October 2018. Goldberg et al. (2019) used operational and modified NO_2 data from May to September 2018, from which only the emissions based on the operational data product are compared. Due to the focus on summer months in Goldberg et al. (2019) and generally lower emissions in summer than in winter (see also section 4.2), lower values are expected in comparison to the two-year average used in this study. For New York the emissions match this expectation. However, for Chicago, Toronto and Colstrip the emissions are comparable or even lower in the two years average than the average over the summer months. A possible explanation is the short averaging period of only one summer and the high variability of NOx emissions, which if not averaged out can potentially lead to a bias. Lorente et al. (2019) used 36 orbits of the operational NO_2 product obtained on 29 different days between February and June 2018 for investigations of emissions for Paris.

https://doi.org/10.5194/acp-2021-273
Preprint. Discussion started: 8 April 2021

Atmospheric Chemistry and Physics Discussions

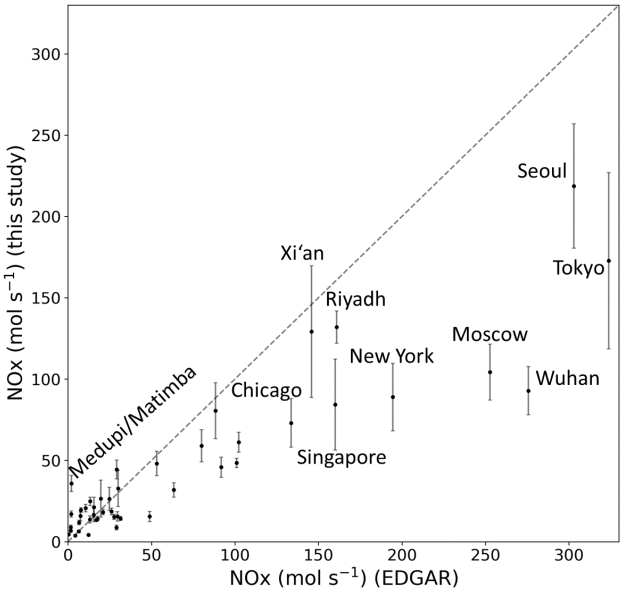

Figure 3. NOx emissions derived from two years of TROPOMI data (01 March 2018 to 29 February 2020) for 45 sources calculated with the EMG method compared to the emissions derived from the EDGAR emission data base (v.5.0, 2015). The dashed line shows the 1:1 ratio. Error bars are 1-sigma uncertainties derived by the EMG fitting procedure for emission estimates.

The comparison of the emissions from the two-year data set show that the emissions of the comparable source regions are

Table 1. NOx emissions for seven source regions compared to the emissions derived by other studies based on TROPOMI data.

Source region	NOx emissions ($\mathrm{mol\,s^{-1}}$)			
	This study	Beirle et al. (2019)	Goldberg et al. (2019)	Lorente et al. (2019)
Riyadh	131.9 ± 5	144.7	—	—
Medupi/Matimba	35.8 ± 2	37.2	—	—
Chicago	73 ± 7	—	73	—
New York	88.9 ± 9	—	57.4	—
Toronto	45.8 ± 3	—	51.9	—
Colstrip	4.2 ± 0.2	—	5.3	—
Paris	48.1 ± 3	—	—	53

overall in good agreement with previous results. Below, the two-year data is presented for a larger set of source regions and separated into shorter time periods to investigate their short-term variability.

https://doi.org/10.5194/acp-2021-273
Preprint. Discussion started: 8 April 2021


Atmospheric Chemistry and Physics Discussions

4.2 Seasonality in emissions

To investigate a possible seasonal variation of NOx emissions, the two years of TROPOMI data are separated into four seasons and emissions are calculated separately for each season. Winter months are from December to February (DJF, southern hemisphere JJA), spring from March to May (MAM, southern hemisphere SON), summer from June to August (JJA, southern hemisphere DJF) and autumn from September to November (SON, southern hemisphere MAM). The two-year data set provides for each season a maximum of two times three months. Due to cloud cover, inhomogeneous wind patterns and resulting partly poor statistics after separating into seasons, only 29 of the 45 source regions are analyzed.

Figure 4 shows the summer-to-winter ratio for these 29 source regions. For most of the source regions, it was found that the emissions are higher during winter months than during summer. Novosibirsk and Krasnoyarsk in Russia and Wuhan in China are among the cities with the lowest summer-to-winter ratio and accordingly clearly higher emissions in winter than during summer. This is expected in places where domestic heating in winter contributes significantly to NOx emissions. The most unexpected ratio is found for Casablanca (Morocco) with a summer-to-winter ratio of 0.28 ± 0.19. Due to the location on the Atlantic coast, which mitigates temperature fluctuations, summers are hot but typically not very hot and winters mild, smaller seasonal variation in emissions is expected. No explanation for this observation could be found so far. For some regions, the emissions are actually higher in summer than in winter like for Medupi/Matimba in South Africa. Interestingly, the regions with a summer-to-winter ratio larger than one or close to one in Saudi Arabia (Riyadh, Rabigh, Tabuk, Buraidah), Libya (Sarir Field) and Sudan (Khartoum) are all located in hot desert climate regions which are dry and warm all year round, but where especially in summer long heat periods are common. A likely explanation is therefore, that the emissions are higher in summer than in winter due to higher power consumption caused by the use of air conditioning in summer. Beirle et al. (2011) reported that the derived emissions are stable throughout the year for Singapore and Madrid, and that variability found for other cities, which could reflect a change in emissions, was not significant. Most other emission studies focused on summer months only and therefore an investigation of seasonality of emissions was not possible (Beirle et al. (2019); Goldberg et al. (2019); Ialongo et al. (2014)). Lorente et al. (2019) found highest emissions on cold weekdays in February and lowest emissions on warm weekend days in spring 2018. Together with comparisons to emission inventories the authors concluded that this indicated the importance of the contributions from the residential heating sector to emissions in winter. Using the full two-year data set, we found a summer-to-winter ratio of 0.46 ± 0.22 for Paris, which supports the results of Lorente et al. (2019).

Overall, the investigation of seasonality shows higher NOx emissions in winter than in summer for the majority of source regions, which is expected due to the location of the majority of the selected regions in mid-latitudes and temperate climate. Not all ratios are significantly different from unity, and some results are unexpected, but the trend from the source regions at high latitudes with higher emissions in winter to the regions in desert climate with higher emissions in summer is plausible.

4.3 Latitudinal and seasonal dependence of lifetimes

Another parameter retrieved by the EMG method is the mean effective lifetime of NOx. Thus, in addition to the seasonality of emissions, the seasonality of lifetimes is investigated as well as their latitudinal dependence.

https://doi.org/10.5194/acp-2021-273
Preprint. Discussion started: 8 April 2021

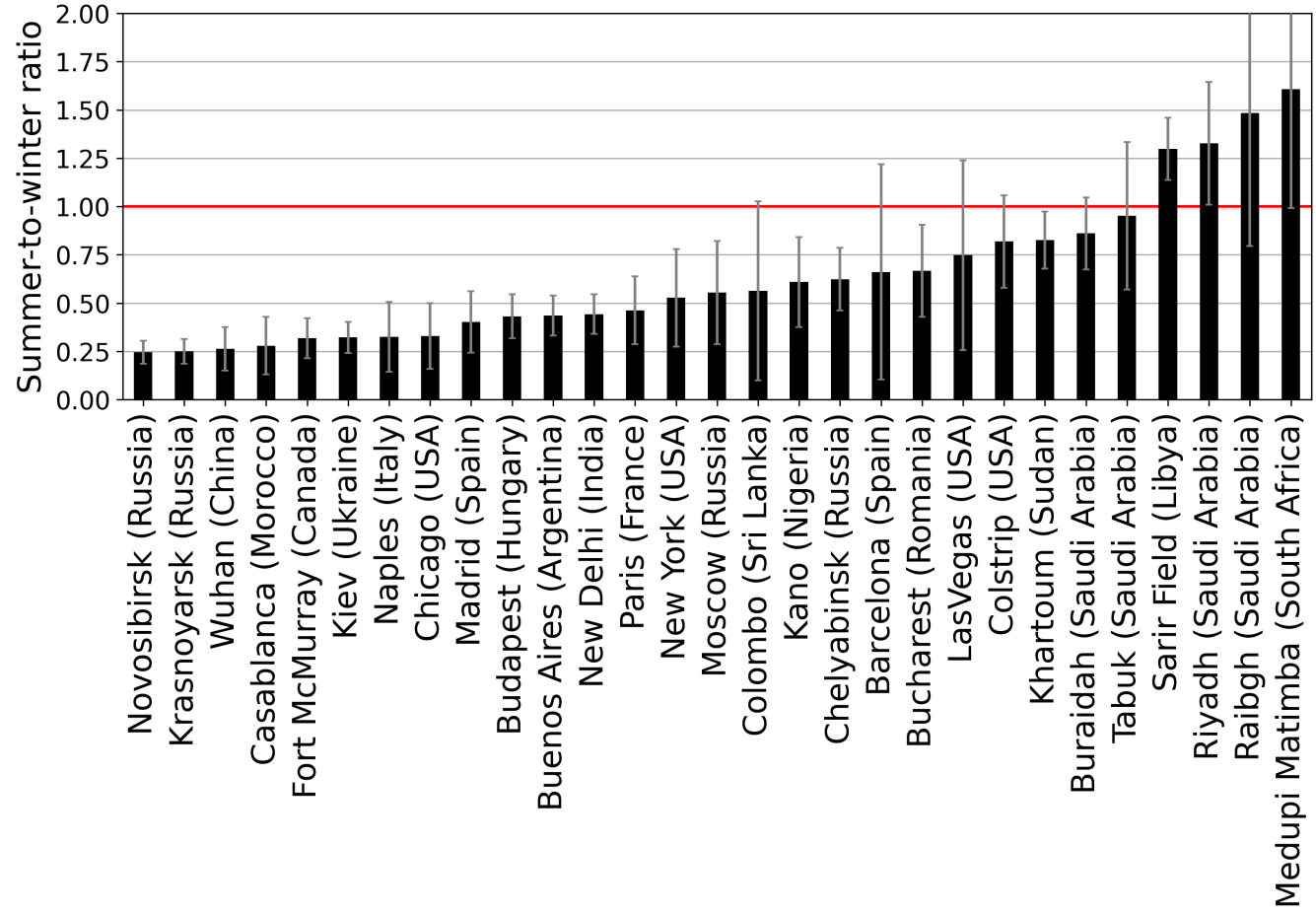

Figure 4. Summer-to-winter ratio for two years of retrieved NOx emission data (01 March 2018 to 29 February 2020). Data were separated into winter (northern hemisphere: DJF, southern hemisphere: JJA) and summer (northern hemisphere: JJA, southern hemisphere: DJF) for 29 source regions. From left to right in increasing ratio. The red line indicates the 1:1 line where summer and winter emissions are equal, below the line winter emissions are larger and over the line the summer emissions are predominant compared to the winter emissions. Error bars are 1-sigma uncertainties derived by the EMG fitting procedure for emission estimates.

Figure 5 (a) shows for the city Madrid the line density in dependence of distance to the source, separated into four seasons. The light blue line is the calculated line density and the blue one the fitted curve for the winter months (DJF). For the two winters (six months) between 01 March 2018 and 29 February 2020, 19 days could be used for the analysis with a mean wind speed on these days of $4.7\,\mathrm{m\,s^{-1}}$. For winter, this results in emissions of $72.0 \pm 7.7\,\mathrm{mol\,s^{-1}}$ and a lifetime of $2.97 \pm 0.33\,\mathrm{h}$. The results for spring (MAM) are shown in green, the summer results (JJA) in red, and the autumn months (SON) are shown in yellow. The calculated lifetimes vary between $2.09 \pm 0.3\,\mathrm{h}$ in autumn and $3.25 \pm 0.3\,\mathrm{h}$ in spring with an average lifetime over the full two years period of $2.75 \pm 0.19\,\mathrm{h}$.

https://doi.org/10.5194/acp-2021-273
Preprint. Discussion started: 8 April 2021


Atmospheric Chemistry and Physics Discussions

This analysis was carried out for all source regions. The averaged lifetimes over the full two-years period for these 45 source regions as a function of latitude are shown in Fig. 5 (b). As a result of the lower sun and thus reduced photolysis and likely lower OH at higher latitudes, one would expect an increase of NOx lifetime with latitude (Martin et al., 2003; Stavrakou et al., 2013). This is broadly confirmed by the results, lifetimes increasing from approximately two hours for source regions at low latitudes near the equator to about eight hours for source regions at high latitudes of around 60 degrees.

The retrieved lifetimes can be used to estimate atmospheric OH concentrations. Assuming that the decay of NOx is determined by the termolecular reaction of OH with NO_2 with the rate constant k_{OH+NO_2+M} for 298 K and 1 atm based on Burkholder et al. (2020), the mean OH concentration ranges from $0.3 \cdot 10^7$ - $1 \cdot 10^7$ molec cm^{-3} for a range of NOx lifetimes of two to eight hours. This is in a reasonable range for OH concentrations at midday (Holland et al., 2003; Smith et al., 2006; Lu et al., 2013).

Figure 5 (c) shows in addition to the two years mean also the lifetimes separated by seasons. As result of the reduced number of data points not all source regions could be included. All seasons show similar latitudinal dependence as described for the mean lifetime but in addition a seasonal dependence is visible with the shortest lifetimes in summer and longer lifetimes in winter. The seasonal differences are small, with the curve of the winter lifetimes starting to deviate more from the other seasons at 25 degrees. Exceptionally long lifetimes are found in winter for Chicago (USA, 41.89° N) with 8.61 ± 2.8 h, Moscow (Russia, 55.95° N) with 8.89 ± 2.97 h and Krasnoyarsk (Russia, 56.1° N) with 10.97 ± 1.93 h. In general, the results are in agreement with values shown in Beirle et al. (2011), where eight different source regions were analyzed yielding lifetimes within a range of two to six hours and a maximum of 8.5 hours during wintertime for Moscow. We can only detect a weak seasonality of the NOx lifetime, which is significantly lower than would be expected from the analyses with GEOS-Chem by Martin et al. (2003) and Shah et al. (2020) which showed lifetimes of about one day in winter compared to around six hours in summer. Possible explanations could be not yet sufficient statistics, a clear-sky bias and also the midday observation time of TROPOMI, which all lead to more balanced lifetimes in summer and winter.

The large data set used in this study reveals a clear but complex latitudinal dependence of NOx lifetimes. This can be used for studies similar to those of Beirle et al. (2019, 2021) where an assumption about the lifetime is necessary to calculate emissions and can also provide relevant observational constraints for model simulations of NOx lifetimes.

4.4 Weekend effect

The presence of a weekend effect in NO_2 on a global scale was first shown by Beirle et al. (2003) with GOME measurements. Anthropogenic activities have their maximum during the week and are reduced during the weekend. Thus, we expect less NOx emissions in cities at weekends. This behavior should be reflected in a comparison of NOx emissions on weekdays and weekends. How large the difference between weekends and weekdays is depends on the types of NOx sources and the different patterns of anthropogenic activity in the source region. To investigate the weekly cycle, the TROPOMI data were separated into week and weekend days and emissions and lifetimes were calculated separately. Weekend days can be one or two days and those days can also differ according to religious tradition. For source regions in Europe and the United States, weekend days were set to be Saturday and Sunday, for Saudi Arabia weekend days are Friday and Saturday (see also Table A1).

https://doi.org/10.5194/acp-2021-273
Preprint. Discussion started: 8 April 2021

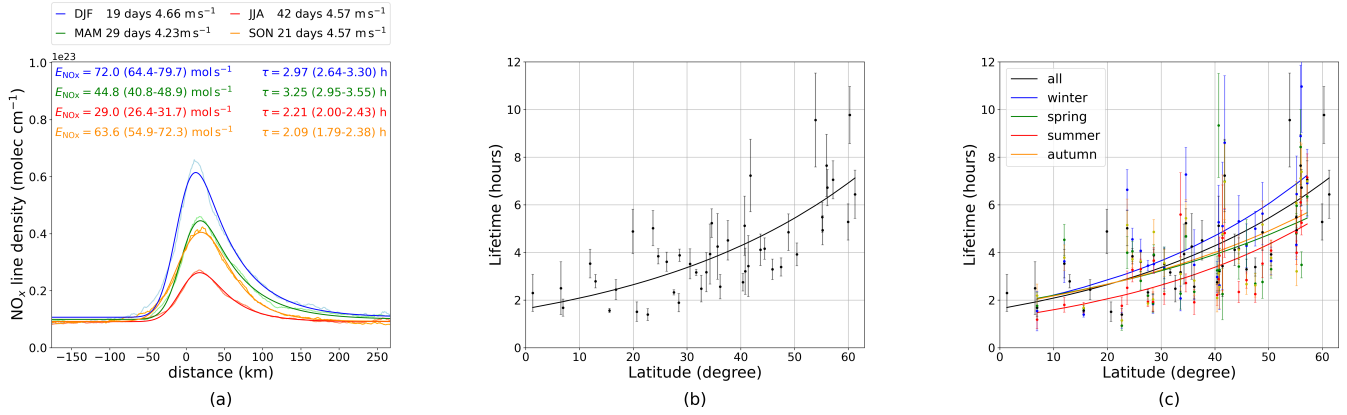

Figure 5. (a) NOx line densities for the city of Madrid separated into seasons for two years of data. The calculated line densities are in light colors and the fit in intense colors. (b) Estimated NOx lifetimes for two years of data for 45 sources as a function of latitude. (c) Estimated lifetimes from two years of data in dependence of latitude (black) separated into winter (blue), spring (green), summer (red) and autumn (yellow). Sources from southern hemisphere are mirrored in latitude and season. Given uncertainties and error bars are 1-sigma uncertainties derived by the EMG fitting procedure.

Figure 6 shows the weekend-to-weekday ratio, with higher emissions during weekdays than on the weekend for most of the source regions albeit with rather high variability. For Paris (France), the emissions are reduced by 38 % on the weekend, which agrees with Lorente et al. (2019). Chicago shows only a reduction of 11 % on the weekend versus weekdays which is less compared to the weekend reductions of 31 % found in Goldberg et al. (2019) for summer 2018.

Source regions not showing any reductions on the weekend are mostly dominated by power plants. Rabigh in Saudi Arabia is a small city with a large gas-fired power plant. Chelyabinsk (Russia) is a city with nearly 1.2 million inhabitants but also a center of heavy industry. Sarir Field is a large oil field in Libya. Hassi Messaud in Algeria is an oil refinery town. Fort McMurray is in the oil sands region in northeastern Alberta, Canada and Medupi/Matimba are two large coal fired power plants in South Africa. Source regions with less industry, which are dominated by domestic and transport emissions like Madrid (Spain) or Paris (France) on the other hand show large emission reductions on the weekend of 43 % and 38 %.

Despite showing large NO_2 columns, Chinese cities do not show a weekend effect in previous studies (Beirle et al., 2003; Stavrakou et al., 2020). Stavrakou et al. (2020) showed an average weekend-to-weekday ratio in NO_2 column over all large Chinese cities of 0.97 ± 0.02 using 2005 - 2017 OMI NO_2 columns and one year of TROPOMI NO_2 columns (May 2018 - April 2019). Ratios of NO_2 columns are related but not identical to ratios in NOx emissions as discussed here, as effects from meteorology and lifetime are not accounted for. Using the EMG method to investigate the weekly cycle we calculated a weekend-to-weekday ratio of 0.78 ± 0.26 in NOx emissions for Wuhan (China). The ratio includes 24 weekend days and 51 weekdays during the period March 2018 - February 2020. Due to the small number of isolated point sources and because of the limited statistics from using two years of data it was not yet possible to determine weekly cycles for other Chinese cities. The ratio for Wuhan indicates a reduction of emissions on rest days also in China in the recent years, in contrast to earlier studies

https://doi.org/10.5194/acp-2021-273
Preprint. Discussion started: 8 April 2021

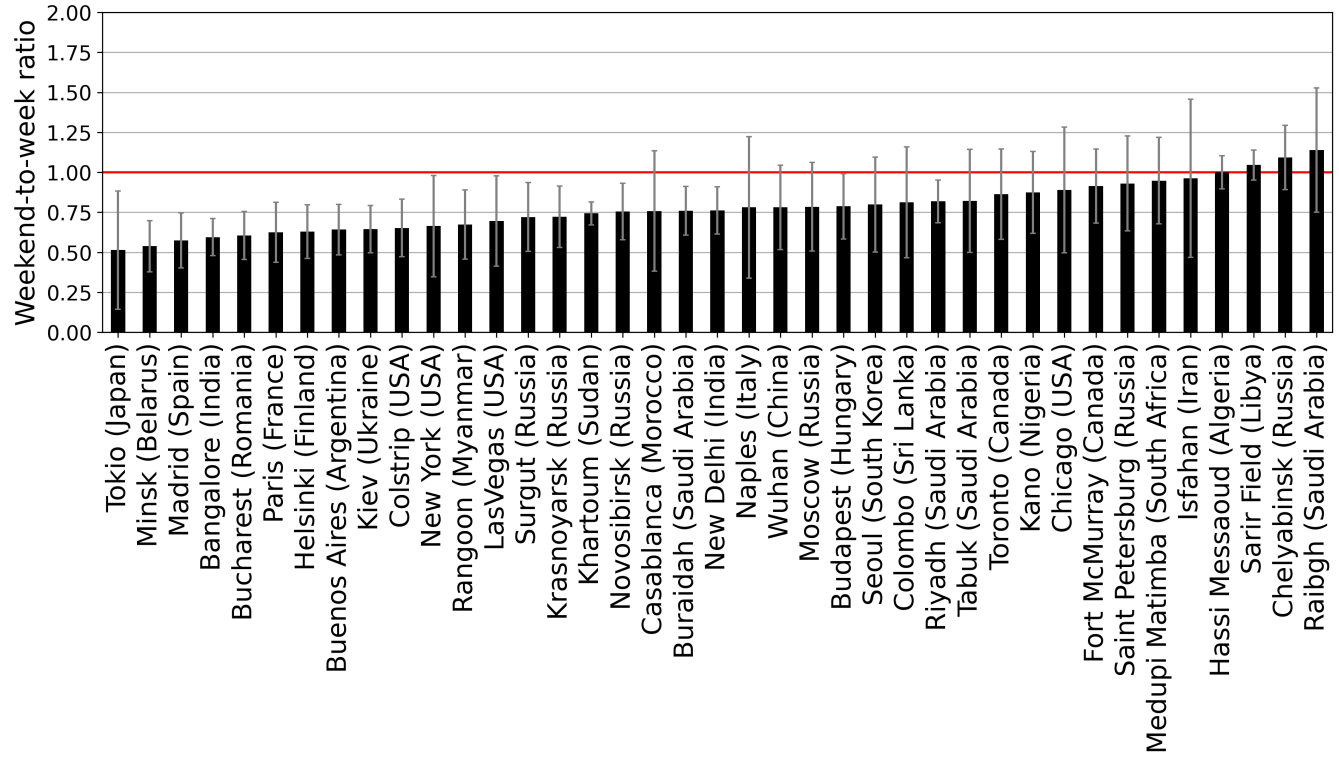

Figure 6. Weekend-to-weekday ratio for two years of NOx emission data (01 March 2018 to 29 February 2020). From left to right in increasing ratio. Data were separated into working and weekend days for 40 source regions. Weekend can be one or two days and those days can also differ according to religious tradition, which is considered. The red line indicates the 1:1 line where weekend and week emissions are equal, below the line emissions during the week are predominant and above the line weekend emissions are higher. Error bars are 1-sigma uncertainties derived by the EMG fitting procedure for emission estimates.

showing no such effect. This can be analyzed in more detail as more TROPOMI data become available.

A side effect of the reduced emissions on weekends could be lower OH levels due to the NO + HO_2 reaction and therefore longer NOx lifetimes (Stavrakou et al., 2008). However, in our data set the retrieved lifetimes for week and weekend days do not show a clear enhancement of lifetimes on weekends (see Fig. A1). This may possibly be due to insufficient number of data points, required for a statistically significant result and should be revisited once a larger TROPOMI data set becomes available.

4.5 Covid-19 effect

In early 2020, several countries took containment measures against the spread of the coronavirus outbreak (Covid-19), which caused reductions in industrial activities and traffic volume. Due to the link of NOx emissions to human activities, it is possible to investigate the impact of the Covid-19 induced activity reductions with the TROPOMI NO_2 column data (Bauwens et al., 2020; Liu et al., 2020; Goldberg et al., 2020). Part of the observed decreases in the NO_2 columns may result from effects

https://doi.org/10.5194/acp-2021-273
Preprint. Discussion started: 8 April 2021


Atmospheric Chemistry and Physics Discussions

other than the measures designed to limit transmission of Covid-19, e.g. meteorological variability, seasonal variability or environmental policy regulations. Consequently, it is problematic to identify a clear Covid-19 effect using only NO_2 column amounts. Besides the possibility of using models to separate the Covid-19 effect from other factors (Goldberg et al., 2020), it is also possible to use the EMG method. This approach accounts for wind conditions and NOx lifetime, which influence the NO_2 columns observed for similar NOx emissions. Since the EMG method can only be used to investigate point sources, the range of possible study areas is limited. We focused on the cities Buenos Aires (Argentina), New Delhi (India) and Madrid (Spain), which are considered to be point sources and have an appropriate number of days with satellite data available during the comparative periods. The EMG method was used, and monthly means of emissions from 2019 and 2020 were calculated and compared.

Figure 7 shows the monthly means from January to November of the calculated NOx emissions of TROPOMI data for 2019 and 2020 for (a) Buenos Aires (b) New Delhi and (c) Madrid. The same months in 2019 and 2020 are compared, as well as the pre Covid-19 period with the period of containment measures. However, in the latter case, seasonality of NOx emissions must be considered. The NOx emissions retrieved for Buenos Aires show lower emissions during summer from January to March (months 1-3), are increasing towards the winter months with a maximum in July and decreasing again towards summer. The emissions for New Delhi do not show such a strong seasonality as those for Buenos Aires but in general the emissions are also higher during the winter months January and February (months 1-2) and decrease towards the summer months. The seasonality is also clearly visible for Madrid, which must be considered in possible comparisons.

On 20 March 2020, a strong nationwide lockdown began in Argentina and lasted in Buenos Aires for more than seven months, ending on 8 November. From January to March, NOx emissions from 2020 are comparable with those from the same months in 2019. In April 2020, the first complete month in lockdown, the emissions are 60 % lower than in April 2019, and also in May 2020, the emissions are 40 % reduced compared to 2019. In June, however, emissions are higher in 2020 than in 2019, although there has been no major change in the containment measures by the government. A possible explanation is that already the June 2019 emissions are lower than expected from the seasonal cycle comparing to May and July 2019. It is also possible that June 2020 emissions are unexpectedly high due to a cold winter month and additional emissions from heating. The emissions in July behave in a manner similar to those in March and April, only with a somewhat smaller decrease of 33 % compared to 2019, similar for September with reductions of 50 %. For August and October emissions are almost equal for both years but in November 2020 they are higher than in 2019, possibly due to the end of lockdown on 8 November.

In India, a nationwide strict lockdown started on 24 March 2020. In January and February, the calculated NOx emissions are higher in 2020 than in 2019. There is no impact of Covid-19 yet in this period, and India's fast-growing economy is probably the explanation for the upward trend in NOx emissions. In April 2020, the first complete month in lockdown, the emissions are 88 % lower than in April 2019, and also in May and June the emissions are with 59 % and 28 % much lower than in 2019. For July to September, comparisons are not possible as less than three days of measurements per month are available due to cloud coverage. In October and November 2020, emissions are almost back to 2019 levels, but without exceeding them, as it was the case at the beginning of the year.

In Europe Madrid was one of the strongly effected cities. A strict lockdown was enacted on 14 March 2020 which lasted until

https://doi.org/10.5194/acp-2021-273
Preprint. Discussion started: 8 April 2021

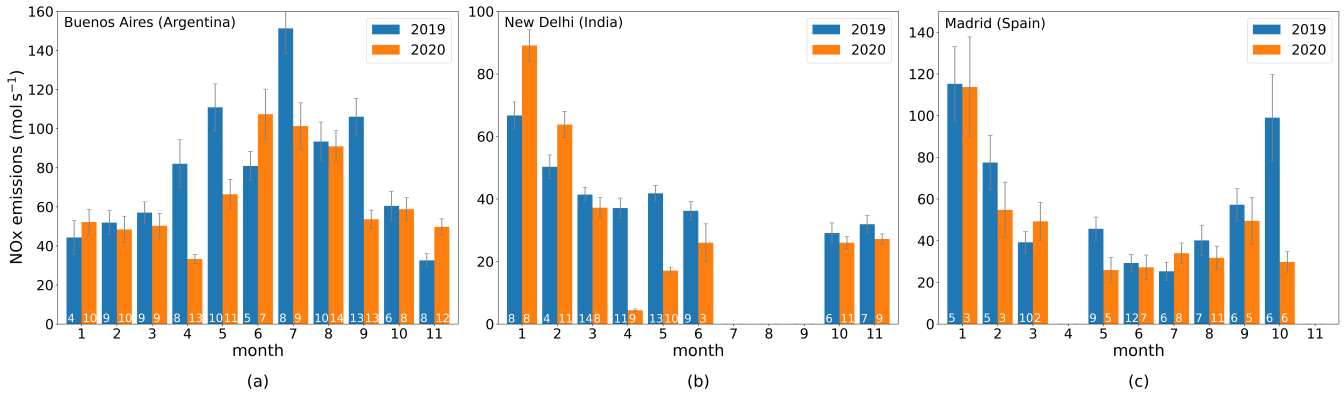

Figure 7. Monthly NOx emissions calculated with the EMG method based on TROPOMI data for 2019 (blue) and 2020 (orange) from January to November for (a) Buenos Aires (Argentina), (b) New Delhi (India) and (c) Madrid (Spain). The numbers in the bars represent the number of available days for the monthly mean. Due to insufficient data availability of less than three days, comparisons are not possible for some months. Error bars are 1-sigma uncertainties derived by the EMG fitting procedure for emission estimates.

June. Due to again rising cases, a second lockdown started in early October 2020. Emission comparisons are not possible for April and November due to lack of data caused by cloud coverage. For the months May and October 2020, when Madrid was in lockdown, the calculated NOx emissions are 43 % respectively 70 % lower than in 2019. This is comparable to results from NO_2 column comparisons which showed reduction of around 30 % from mid of March to early April 2020 relative to 2019 (Bauwens et al., 2020). However, even with monthly averages, the high variability of NOx emissions is still not negligible, which may be a reason for the high deviation from the retrieved emissions for October 2019 compared to previous months.

Despite the shortness of the periods available for analysis, it is possible to investigate short-term variability of NOx emissions induced by Covid-19 with TROPOMI NO_2 data and the EMG method. Strong decreases due to lockdown measures of 60 % in Buenos Aires and 88 % in New Delhi are shown for April 2020 compared to April 2019, as well as a general tendency towards lower emissions in 2020 after the start of the Covid-19 pandemic than 2019. Nevertheless, even with monthly averages, the high variability of NOx must still be considered for particular months. These emission estimates account for wind conditions and NOx lifetime and can therefore give a better estimate of the Covid-19 measures on NOx emissions than just comparing NO_2 column measurements. For some cities and months, the number of days in monthly means is limited due to cloud cover. This is also a problem when comparing monthly NO_2 column levels.

4.6 Uncertainties

The uncertainties and error bars for emission and lifetime estimates given in this work are based on 1-sigma uncertainties (standard deviation), derived by the fitting procedure and are calculated with error propagation. For emissions this results in:

$$\sigma_E = \frac{\overline{w} \cdot \sigma_{\mathrm{E'}}}{N_\mathrm{A}} + \frac{E' \cdot \sigma_{\overline{w}}}{N_\mathrm{A}} \tag{13}$$

https://doi.org/10.5194/acp-2021-273
Preprint. Discussion started: 8 April 2021


Atmospheric Chemistry and Physics Discussions

and for lifetimes in:

$$\sigma_\tau = \frac{\sigma_{x_0}}{\overline{w}} + \frac{x_0 \cdot \sigma_{\overline{w}}}{\overline{w}^2} \tag{14}$$

with the emission factor E', the e-folding distance x_0, the mean wind speed $\overline{w}$, the Avogadro's constant N_A (see section 2) and the standard deviations $\sigma_{\mathrm{E}'}$ of E' and σ_{x_0} of x_0 derived from the fit and $\sigma_{\overline{w}}$ derived from the wind field in the line density sector. These estimates are based on the fitting uncertainties. However, the NOx emissions and lifetimes derived from TROPOMI NO_2 data are influenced by additional error sources. The most important contribution directly influencing our estimates is the accuracy of the TROPOMI NO_2 tropospheric vertical column itself. This uncertainty is dominated by the accuracy of the tropospheric air mass factor (AMF) and is estimated to be in the order of 30 % (Boersma et al., 2004, Bucsela et al., 2013). Recent studies comparing TROPOMI NO_2 column with co-located ground based or aircraft measurements reported a low bias for TROPOMI NO_2 columns, which is most likely caused by a-priori information such as the surface albedo, cloud-top-height, cloud fraction and the NO_2 vertical profile, used for tropospheric AMF calculations. This bias differs for different regions and is more pronounced for regions with larger NO_2 columns (Griffin et al., 2019; Ialongo et al., 2020; Judd et al., 2020; Dimitropoulou et al., 2020; Verhoelst et al., 2021). Some studies scaled up the measured NO_2 columns with a factor of 1.33 for Paris (Lorente et al., 2019) up to a factor of 1.98 for Germany (Beirle et al., 2019). As this suspected underestimation is not yet fully characterized, and as it is not clear without independent measurements how much the various regions used in our study are affected, we decided not to correct the operational product. It is therefore probable that the NOx emissions derived in this study are biased low.

To calculate NOx emissions, we applied a conversion of each TROPOMI pixel from NO_2 column to NOx column by assuming that the Leighton photostationary state applies for the polluted air masses. This is more accurate than using a fixed conversion factor, especially for our analysis over a large latitudinal range and for different seasons. Nevertheless, the photolysis frequencies have to be parameterized and the temperatures for the rate constant and the ozone concentrations taken from the monthly CAMS reanalysis data set interpolated to a mean early afternoon S5P overpass time. Thus, the conversion from NO_2 to NOx adds uncertainties in the emission estimates.

In addition, using satellite data introduces a clear-sky bias, because only measurements from nearly cloudless days are used, which favor specific emission patterns. These may differ from those of cloudier and thereby often cooler days. The limitation to nearly cloudless measurements also influence lifetime estimates, which are systematically lower due to higher photolysis rates on cloudless days. Furthermore, the retrieved NOx emissions and lifetimes are based on measurements in the early afternoon and are therefore biased due to the measurement time. The variability in time can be further analyzed using follow-up sensors on geostationary satellites as for example GEMS, Tempo or Sentinel-4.

The NO_2 tropospheric columns are strongly affected by the wind fields. This affects the calculation of NOx emissions and lifetimes. We filtered the NO_2 measurements depending on the corresponding wind speed and only data with wind speeds > $2\,\mathrm{m\,s^{-1}}$ are included in the analysis. As a result of the short lifetime of NO_2, the observed NO_2 distribution should, in general, be dominated by the wind conditions around the satellite overpass. On days with rapidly changing wind directions around the time of measurement, the spatial patterns and thus the estimates of emissions and lifetimes may be affected. An effect observed

https://doi.org/10.5194/acp-2021-273
Preprint. Discussion started: 8 April 2021


Atmospheric Chemistry and Physics Discussions

for some locations on some days are curved plumes, which for the case of strong curvature leads to a part of the plume being outside of the line density calculation sector and an underestimation of both NOx emission and lifetime. This has a large effect when analyzing estimates for single days. It has a smaller influence on the overall result analyzing a larger average, if not too many days are affected by rapidly changing wind directions. Nevertheless, the wind field is the largest uncertainty influencing our estimates after the NO_2 column itself. Lorente et al. (2019) have modified wind speeds by 20 % and found that emissions changed by 20 %, which demonstrates the strong influence of wind speed on NOx emissions. However, reliable global wind information is hard to obtain. Beirle et al. (2011) estimated an uncertainty of 30 % for the wind data. The uncertainties due to the chosen wind fields will vary for different source regions. Overall, we consider an uncertainty of 30 %.

To avoid interference from sources of NOx surrounding the target region, only rather isolated source regions are chosen for the analysis. Since almost no site is perfectly isolated, sectors were defined in which the line density was calculated by integration and fitted with the EMG method to minimize interference between different sources. Due to the rotation of measurements with their corresponding wind direction around the source, the NO_2 signal from sources in the surroundings is smeared around the source region in their distance to the source location. To exclude these contaminants, the sector size used for the EMG method has to be chosen carefully. In order to have an adequate amount of data for a robust EMG fit, the sector must first be large enough in both downwind and across-wind directions, but the size is also influenced by other factors. The sector length in wind direction is mainly determined by the influence of other sources but also the spatial extent of the source region itself and wind speeds. A typical size is 300 km, 100 km upwind and 200 km downwind of the source location and is adjusted visually, if necessary, by inspecting the NO_2 distribution and line density. If the influence of surrounding sources is negligible or becomes negligible by adjusting the sector size, the EMG method is robust in variation of the sector size in wind direction. The sector width in across-wind direction is mainly influenced by the geographical extent of the source region. If the sector width is chosen too small, part of the NOx emissions are outside of the sector due to dilution by wind or due to curved plumes, as described above. This obviously leads to an underestimation of the calculated emissions which acts as an additional apparent loss, leading to the e-folding distance x_0 being biased low and also lifetimes, defined as $\tau = x_0 \cdot w^{-1}$, with mean wind speed w, are underestimated. Typical sector widths vary between 30 km to 140 km and are determined by visually inspecting the NO_2 distribution after rotation. Beirle et al. (2019) estimated the uncertainty of NOx emissions and lifetimes due to sector size to 10 %.

The EMG method is well suited to investigate point sources. In reality, most of the analyzed sources deviate from the assumption of a point source. Isolated sources as the power plant Colstrip in Montana, USA or Sarir Oil Field in Libya are close to being point sources. In previous studies, the Four Corners and San Juan power plants in New Mexico, USA, which are located 13 km apart, were investigated as one source using the EMG method (Beirle et al., 2011; Goldberg et al., 2019). With the higher resolution of TROPOMI compared to OMI, it becomes clear that the situation with the two plumes is more complex. This is evidenced by strong irregularities in the line density and fit, indicating that it should not be treated as one point source. Other sources such as Tokyo, Moscow or Chicago, all cities with emissions originating from a larger area, are treated as extended point sources but additional uncertainties must be considered. For example, it is not possible to consider a change of the instantaneous NOx lifetime downwind of the source with the EMG method and estimated lifetimes should be interpreted

https://doi.org/10.5194/acp-2021-273
Preprint. Discussion started: 8 April 2021


Atmospheric Chemistry and Physics Discussions

as an effective mean lifetime (Beirle et al., 2011). This effect is particularly pronounced in spatially extended source areas and can lead to low biased lifetimes.

In summary, the total uncertainty of NOx emissions and lifetimes derived from TROPOMI NO_2 data is influenced by different error sources but mostly by the uncertainties in the TROPOMI NO_2 tropospheric column itself (30 % - 50 %) and in the wind field (30 %). The sector size can lead to low biased emissions and lifetimes and is estimated to introduce an uncertainty of 10 %. Further uncertainties due to the measurement time, the clear-sky bias and assumptions about point sources tend to have low bias in the lifetimes and emissions. More analysis is needed to resolve these issues. The error contributions summed in quadrature result in an overall uncertainty estimate for lifetime and emissions in the range 43 % - 62 %.

5 Conclusions

In this study, we present investigations of the variability of NOx emissions and lifetimes estimated from Sentinel-5P TROPOMI observations for selected urban areas around the world. Similar to earlier studies, we combine TROPOMI NO_2 tropospheric vertical column data with wind information from ECMWF ERA5 reanalysis for the exponentially modified Gaussian, EMG, method. TROPOMI measurements with their high spatial resolution and high signal to noise ratio allow detailed analysis of NOx emissions and lifetimes using only two years of data. Investigating small emission sources not analyzed before and also monitoring the variability on a short-term temporal basis has been possible. Here, a total of 45 NOx sources from different regions, located between the equator and 61° latitude are investigated.

The resulting emission estimates are compared to the EDGAR (v.5.0 2015) emission inventory, showing higher emissions for most of the source regions in the EDGAR database than estimated with the EMG method. These differences are particularly strong for the source regions with the highest emissions. Comparisons to other studies using TROPOMI data and similar methods for emission estimates show smaller differences and in general good agreement. As the operational TROPOMI tropospheric NO_2 product has been reported to be low in comparison to independent measurements, part of the apparent overestimation by EDGAR could be related to a TROPOMI low bias. On the other hand, NOx emission reductions over the last five years are likely to also have an impact.

The seasonal separation of the emission estimates in general shows the highest emissions during winter and a trend from source regions at higher latitudes with higher emissions in winter, to regions in hot desert climate with higher emissions in summer. This is best explained by the different contributions to NOx emissions depending on source region, which are typically dominated by domestic heating in winter or, air conditioning in hot summer months, depending on the climatic conditions of the source region. The investigation of the seasonal and latitudinal dependence of the NOx lifetime shows an increase in lifetime from two to six hours in correlation to an increase in latitude, but only a weak seasonal dependence with longer lifetimes in winter than in summer.

Separating NOx emission estimates into working and weekend days indicates that for most NOx source regions, emissions are higher during weekdays than on the weekend, albeit with rather high variability in the weekend-to-weekday ratios. Only source regions, which are dominated by power plants or industry, do not show any reductions in NOx emissions on the weekend. The

https://doi.org/10.5194/acp-2021-273
Preprint. Discussion started: 8 April 2021


Atmospheric Chemistry and Physics Discussions

largest emission reductions on weekends are found for source regions with little industry, which are dominated by city emissions mostly from traffic. Our results indicate reductions of NOx emissions for Wuhan (China) during weekends, in contrast to earlier studies showing no such effect in China. This study can be extended to other Chinese cities, as more high resolution tropospheric NO_2 columns become available from TROPOMI and GEMS in the next years. Separately calculated lifetimes for weekend and working days do not show longer lifetimes during weekends. This result also requires further investigation.

A short-term reduction in emissions attributable to the measures introduced to limit the spread of Covid-19 infections was found by comparing NOx emissions estimated with the EMG method. Since the method accounts for wind conditions and NOx lifetimes, it gives a better estimate on the impact of the Covid-19 measures on NOx emissions than comparisons of tropospheric NO_2 column measurements as done in other studies. Strong NOx emission reduction during the first lockdown phase and a general tendency to lower emissions in 2020 than in 2019 is shown for Buenos Aires, New Delhi and Madrid.

We conclude that the EMG method in combination with the high-resolution TROPOMI NO_2 measurements allows us to investigate the high variability of NOx emissions and lifetimes on a global scale and on short time frames. The ability to estimate emissions over short time periods will also allow policy makers to evaluate NOx emission regulations better and more quickly. The presented high variability should be further investigated using follow-up sensors on geostationary satellites as for example GEMS, Tempo or Sentinel-4, which have the potential to investigate in addition the diurnal variability.

https://doi.org/10.5194/acp-2021-273
Preprint. Discussion started: 8 April 2021

Atmospheric Chemistry and Physics Discussions

Appendix A

Table A1. NOx source regions sorted with increasing latitude with mean NOx lifetime and emission, wind speed, available days, season flag and weekly cycle flag (x: possible, –: not possible).

Source region	Latitude (degree)	Longitude (degree)	NOx lifetime (hours)	NOx emission (mol s^{-1})	wind speed (m s^{-1})	days	seasons	weekdays
Singapore (Singapore)	1.30	103.69	2.3 ± 0.39	84.3 ± 14.0	4.75	14	–	–
Lagos (Nigeria)	6.55	3.40	2.5 ± 0.55	26.5 ± 5.7	4.01	23	–	–
Colombo (Sri Lanka)	6.93	79.85	1.68 ± 0.18	15.5 ± 1.6	4.98	53	x	Sat, Sun
Kano (Nigeria)	11.98	8.51	3.53 ± 0.3	3.8 ± 0.3	3.80	259	x	Sat, Sun
Bangalore (India)	12.98	77.59	2.79 ± 0.14	14.3 ± 0.6	3.83	117	–	Sun
Khartoum (Sudan)	15.58	32.52	1.56 ± 0.05	13.3 ± 0.3	5.10	473	x	Fri, Sat
Rangoon (Myanmar)	16.78	96.15	2.44 ± 0.21	13.6 ± 1.1	3.34	79	–	Sat, Sun
Belo Horizonte (Brazil)	19.91	-43.98	4.88 ± 0.46	8.7 ± 0.7	3.29	39	–	–
Guadalajara (Mexico)	20.66	-103.34	1.51 ± 0.2	26.3 ± 3.6	4.29	122	–	–
Raibgh (Saudi Arabia)	22.69	39.03	1.39 ± 0.13	59.0 ± 5.0	5.51	303	x	Fri, Sat
Medupi Matimba (South Africa)	23.68	27.58	5.02 ± 0.37	35.8 ± 2.5	4.18	151	x	Sat, Sun
Riyadh (Saudi Arabia)	24.65	46.71	3.84 ± 0.16	131.9 ± 4.9	5.21	316	x	Fri, Sat
Buraidah (Saudi Arabia)	26.20	43.99	3.61 ± 0.2	18.2 ± 0.8	4.68	398	x	Fri, Sat
Sarir Field (Libya)	27.55	21.63	2.32 ± 0.06	4.5 ± 0.1	4.99	411	x	Fri, Sat
Tabuk (Saudi Arabia)	28.48	36.52	1.89 ± 0.19	15.8 ± 1.5	4.72	245	x	Fri, Sat
New Delhi (India)	28.62	77.22	3.88 ± 0.13	48.4 ± 1.4	4.24	165	x	Sun
Wuhan (China)	30.57	114.28	3.52 ± 0.32	92.8 ± 7.4	4.23	75	x	Sat, Sun
Hassi Messaoud (Algeria)	31.70	6.05	3.16 ± 0.06	6.7 ± 0.1	5.35	360	–	Fri, Sat
Isfahan (Iran)	32.64	51.67	2.48 ± 0.28	80.5 ± 8.6	4.65	105	–	Fri
Casablanca (Morocco)	33.59	-7.61	3.17 ± 0.41	16.6 ± 2.1	4.37	253	x	Sat, Sun
Xi'an (China)	34.27	108.94	3.93 ± 0.63	129.2 ± 20.2	4.20	17	–	–
Buenos Aires (Argentina)	34.60	-58.38	5.23 ± 0.3	61.1 ± 3.0	5.40	187	x	Sat, Sun
Tokyo (Japan)	35.68	139.77	4.25 ± 0.69	172.8 ± 27.1	5.83	23	–	Sat, Sun
Las Vegas (USA)	36.16	-115.19	2.56 ± 0.26	15.5 ± 1.5	5.14	188	x	Sat, Sun
Seoul (South Korea)	37.60	127.00	4.51 ± 0.42	218.7 ± 19.2	5.08	104	–	Sat, Sun
Madrid (Spain)	40.41	-3.70	2.75 ± 0.18	44.4 ± 2.9	4.51	110	x	Sat, Sun
New York (USA)	40.71	-74.01	5.12 ± 0.62	88.9 ± 10.3	5.88	120	x	Sat, Sun
Naples (Italy)	40.83	14.25	3.21 ± 0.49	21.2 ± 3.0	5.36	86	x	Sat, Sun
Barcelona (Spain)	41.40	2.17	3.43 ± 0.64	32.8 ± 5.5	5.93	41	x	–

https://doi.org/10.5194/acp-2021-273
Preprint. Discussion started: 8 April 2021

Atmospheric Chemistry and Physics Discussions

Table A2. Continuation of table A1

Source region	Latitude (degree)	Longitude (degree)	NOx lifetime (hours)	NOx emission (mol s^{-1})	wind speed (m s^{-1})	days	seasons	weekdays
Chicago (USA)	41.80	-87.80	7.23 ± 0.76	73.0 ± 7.4	6.05	74	x	Sat, Sun
Toronto (Canada)	43.66	-79.38	4.11 ± 0.33	45.8 ± 3.1	5.40	61	–	Sat, Sun
Bucharest (Romania)	44.43	26.10	4.16 ± 0.23	6.3 ± 0.3	4.34	114	x	Sat, Sun
Colstrip (USA)	45.88	-106.61	3.29 ± 0.21	4.2 ± 0.2	5.38	149	x	Sat, Sun
Budapest (Hungary)	47.50	19.05	3.39 ± 0.19	14.1 ± 0.7	4.58	122	x	Sat, Sun
Paris (France)	48.86	2.35	4.85 ± 0.38	48.1 ± 3.7	4.91	105	x	Sat, Sun
Kiev (Ukraine)	50.45	30.50	3.92 ± 0.24	20.6 ± 1.2	4.81	133	x	Sat, Sun
Minsk (Belarus)	53.90	27.55	9.56 ± 0.98	11.8 ± 0.7	5.45	121	–	Sat, Sun
Novosibirsk (Russia)	55.15	82.98	5.48 ± 0.32	24.8 ± 1.3	5.26	97	x	Sat, Sun
Chelyabinsk (Russia)	55.21	61.44	4.93 ± 0.31	19.5 ± 0.8	5.31	95	x	Sat, Sun
Moscow (Russia)	55.95	37.62	7.65 ± 0.65	104.3 ± 8.6	5.20	61	x	Sat, Sun
Krasnoyarsk (Russia)	56.10	92.93	6.72 ± 0.38	15.2 ± 0.8	4.46	87	x	Sat, Sun
Fort McMurray (Canada)	57.17	-111.59	7.05 ± 0.4	17.0 ± 0.9	4.65	88	x	Sat, Sun
Saint Petersburg (Russia)	59.95	30.40	5.28 ± 0.38	31.8 ± 2.2	5.16	72	–	Sat, Sun
Helsinki (Finland)	60.29	24.96	9.77 ± 0.6	18.6 ± 1.1	5.78	81	–	Sat, Sun
Surgut (Russia)	61.25	73.43	6.44 ± 0.51	8.8 ± 0.7	5.56	68	–	Sat, Sun

https://doi.org/10.5194/acp-2021-273
Preprint. Discussion started: 8 April 2021

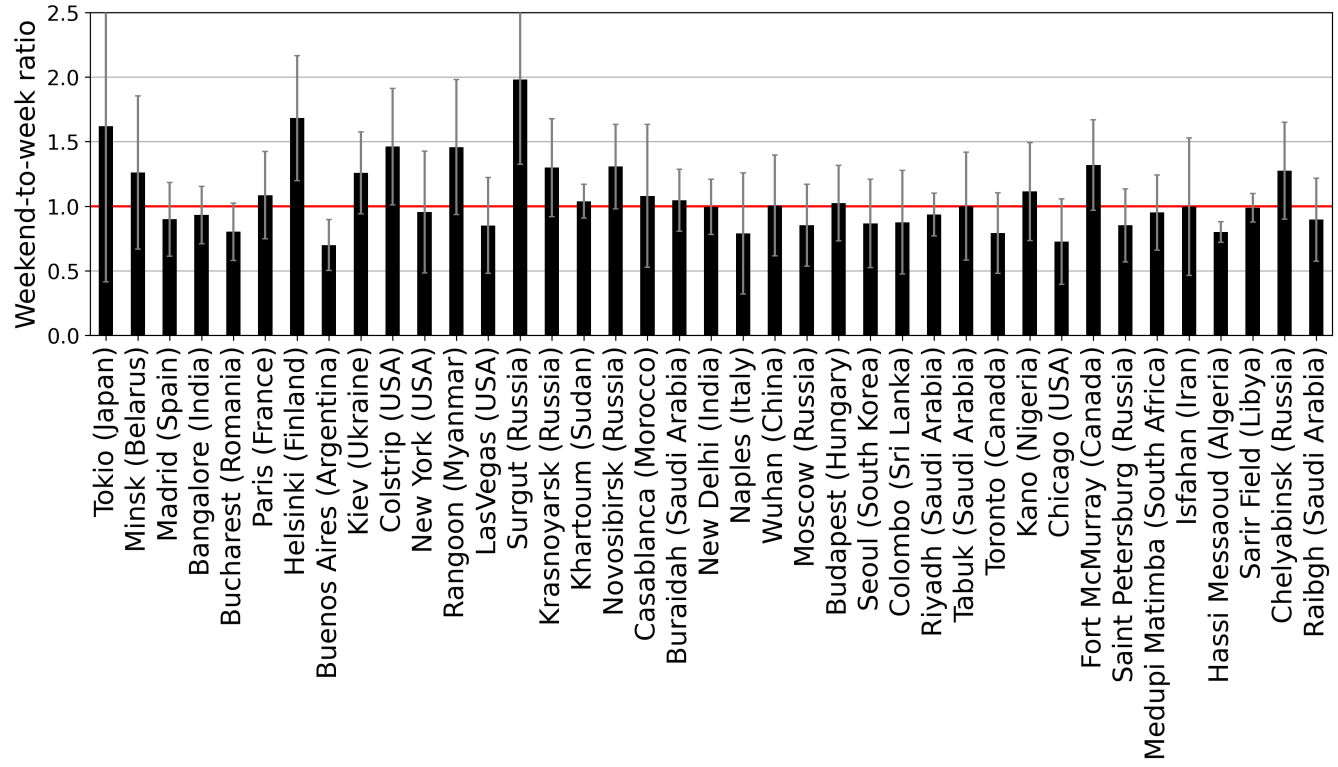

Figure A1. Weekend-to-weekday ratio for two years of NOx lifetimes (01 March 2018 to 29 February 2020). From left to right in increasing weekend-to-weekday NOx emission ratio (see Fig. 6). Data were separated into working and weekend days for 40 source regions. Weekend can be one or two days and those days can also differ according to religious tradition, which is considered. The red line indicates the 1:1 line where weekend and weekday lifetimes are equal, below the line weekday lifetimes are longer and over the line weekend lifetimes are longer. Error bars are 1-sigma uncertainties derived by the EMG fitting procedure for lifetime estimates

https://doi.org/10.5194/acp-2021-273
Preprint. Discussion started: 8 April 2021

Atmospheric Chemistry and Physics Discussions

Data availability. TROPOMI data from July 2018 onwards are freely available via https://s5phub.copernicus.eu/. The 100-m wind from the ERA5 reanalysis is freely available from the Copernicus Climate Change (C3S) climate data store (CDS) (http://doi.org/10.24381/cds.adbb2d47). The CAMS reanalysis EAC4 data were provided by ECMWF and are freely available https://ads.atmosphere.copernicus.eu/cdsapp#!/search?type=dataset. EDGAR v5.0 Global Air Pollutant Emissions are available by https://edgar.jrc.ec.europa.eu/overview.php?v=50_AP.

Author contributions. KL, AR and JPB designed the study. KL performed the analysis and wrote the paper with contributions from JPB and AR.

Competing interests. The authors declare that they have no conflict of interest.

Acknowledgements. We gratefully acknowledge the German Aerospace Center (DLR) Bonn for funding the MAXGRAD project – project no. 50 EE 1709A. Copernicus Sentinel-5P level 2 NO_2 data are used in this study. Sentinel-5 Precursor is a European Space Agency (ESA) mission on behalf of the European Commission (EC). The TROPOMI pay-load is a joint development by ESA and the Netherlands Space Office (NSO). The Sentinel-5 Precursor ground-segment development has been funded by ESA and with national contributions from the Netherlands, Germany, Belgium, and UK. ERA5 reanalysis wind data were provided by ECMWF. The CAMS reanalysis EAC4 data were provided by ECMWF. EDGAR v5.0 Global Air Pollutant Emissions are provided by https://edgar.jrc.ec.europa.eu/overview.php?v=50_AP, DOI: https://data.europa.eu/doi/10.2904/JRC_DATASET_EDGAR.

https://doi.org/10.5194/acp-2021-273
Preprint. Discussion started: 8 April 2021


Atmospheric Chemistry and Physics Discussions

References

Alvarado, L. M., Richter, A., Vrekoussis, M., Hilboll, A., Hedegaard, A. B. K., Schneising, O., and Burrows, J. P.: Unexpected long-range transport of glyoxal and formaldehyde observed from the Copernicus Sentinel-5 Precursor satellite during the 2018 Canadian wildfires, Atmospheric Chemistry and Physics, 20, 2057–2057, 2020.

Atkinson, R., Baulch, D. L., Cox, R. A., Crowley, J. N., Hampson, R. F., Hynes, R. G., Jenkin, M. E., Rossi, M. J., and Troe, J.: Evaluated kinetic and photochemical data for atmospheric chemistry: Volume I - gas phase reactions of O_x, HO_x, NO_x and SO_x species, Atmospheric Chemistry and Physics, 4, 1461–1738, https://doi.org/10.5194/acp-4-1461-2004, https://acp.copernicus.org/articles/4/1461/2004/, 2004.

Bauwens, M., Compernolle, S., Stavrakou, T., Müller, J.-F., Van Gent, J., Eskes, H., Levelt, P., van der A, R., Veefkind, J., Vlietinck, J., et al.: Impact of coronavirus outbreak on NO2 pollution assessed using TROPOMI and OMI observations, Geophysical Research Letters, p. e2020GL087978, 2020.

Beirle, S., Platt, U., Wenig, M., and Wagner, T.: Weekly cycle of NO_2 by GOME measurements: a signature of anthropogenic sources, Atmospheric Chemistry and Physics, 3, 2225–2232, https://doi.org/10.5194/acp-3-2225-2003, https://acp.copernicus.org/articles/3/2225/2003/, 2003.

Beirle, S., Boersma, K. F., Platt, U., Lawrence, M. G., and Wagner, T.: Megacity emissions and lifetimes of nitrogen oxides probed from space, Science, 333, 1737–1739, 2011.

Beirle, S., Borger, C., Dörner, S., Li, A., Hu, Z., Liu, F., Wang, Y., and Wagner, T.: Pinpointing nitrogen oxide emissions from space, Science advances, 5, eaax9800, 2019.

Beirle, S., Borger, C., Dörner, S., Eskes, H., Kumar, V., de Laat, A., and Wagner, T.: Catalog of NO_x emissions from point sources as derived from the divergence of the NO_2 flux for TROPOMI, Earth System Science Data Discussions [preprint], 2021, 1–28, https://doi.org/10.5194/essd-2020-280, https://essd.copernicus.org/preprints/essd-2020-280/, 2021.

Bovensmann, H., Burrows, J., Buchwitz, M., Frerick, J., Noël, S., Rozanov, V., Chance, K., and Goede, A.: SCIAMACHY: Mission objectives and measurement modes, Journal of the atmospheric sciences, 56, 127–150, 1999.

Burkholder, J., Sander, S., Abbatt, J., Barker, J., Cappa, C., Crounse, J., Dibble, T., Huie, R., Kolb, C., Kurylo, M., et al.: Chemical kinetics and photochemical data for use in atmospheric studies; evaluation number 19, Tech. rep., Pasadena, CA: Jet Propulsion Laboratory, National Aeronautics and Space . . . , 2020.

Burrows, J. P., Weber, M., Buchwitz, M., Rozanov, V., Ladstätter-Weißenmayer, A., Richter, A., DeBeek, R., Hoogen, R., Bramstedt, K., Eichmann, K.-U., et al.: The global ozone monitoring experiment (GOME): Mission concept and first scientific results, Journal of the Atmospheric Sciences, 56, 151–175, 1999.

Crippa, M., Guizzardi, D., Muntean, M., Schaaf, E., Dentener, F., van Aardenne, J. A., Monni, S., Doering, U., Olivier, J. G., Pagliari, V., et al.: Gridded emissions of air pollutants for the period 1970–2012 within EDGAR v4. 3.2, Earth Syst. Sci. Data, 10, 1987–2013, 2018.

Crippa, M., Oreggioni, G., Guizzardi, D., Muntean, M., Schaaf, E., Lo Vullo, E., Solazzo, E., Monforti-Ferrario, F., Olivier, J. G., and Vignati, E.: Fossil CO2 and GHG emissions of all world countries, Luxemburg: Publication Office of the European Union, 2019.

de Foy, B., Wilkins, J. L., Lu, Z., Streets, D. G., and Duncan, B. N.: Model evaluation of methods for estimating surface emissions and chemical lifetimes from satellite data, Atmospheric Environment, 98, 66–77, 2014.

de Foy, B., Lu, Z., Streets, D. G., Lamsal, L. N., and Duncan, B. N.: Estimates of power plant NOx emissions and lifetimes from OMI NO2 satellite retrievals, Atmospheric Environment, 116, 1–11, 2015.

https://doi.org/10.5194/acp-2021-273
Preprint. Discussion started: 8 April 2021

Atmospheric Chemistry and Physics Discussions

Dickerson, R. R., Stedman, D. H., and Delany, A. C.: Direct measurements of ozone and nitrogen dioxide photolysis rates in the troposphere, Journal of Geophysical Research: Oceans, 87, 4933–4946, 1982.

Dimitropoulou, E., Hendrick, F., Pinardi, G., Friedrich, M. M., Merlaud, A., Tack, F., De Longueville, H., Fayt, C., Hermans, C., Laffineur, Q., Fierens, F., and Van Roozendael, M.: Validation of TROPOMI tropospheric NO_2 columns using dual-scan multi-axis differential optical absorption spectroscopy (MAX-DOAS) measurements in Uccle, Brussels, Atmospheric Measurement Techniques, 13, 5165–5191, https://doi.org/10.5194/amt-13-5165-2020, https://amt.copernicus.org/articles/13/5165/2020/, 2020.

Dittman, M. G., Ramberg, E., Chrisp, M., Rodriguez, J. V., Sparks, A. L., Zaun, N. H., Hendershot, P., Dixon, T., Philbrick, R. H., and Wasinger, D.: Nadir ultraviolet imaging spectrometer for the NPOESS Ozone Mapping and Profiler Suite (OMPS), in: Earth Observing Systems VII, vol. 4814, pp. 111–119, International Society for Optics and Photonics, 2002.

Georgoulias, A. K., van der A, R. J., Stammes, P., Boersma, K. F., and Eskes, H. J.: Trends and trend reversal detection in 2 decades of tropospheric NO_2 satellite observations, Atmospheric Chemistry and Physics, 19, 6269–6294, https://doi.org/10.5194/acp-19-6269-2019, https://acp.copernicus.org/articles/19/6269/2019/, 2019.

Goldberg, D. L., Lu, Z., Streets, D. G., de Foy, B., Griffin, D., McLinden, C. A., Lamsal, L. N., Krotkov, N. A., and Eskes, H.: Enhanced Capabilities of TROPOMI NO2: Estimating NO X from North American Cities and Power Plants, Environmental science & technology, 53, 12 594–12 601, 2019.

Goldberg, D. L., Anenberg, S. C., Griffin, D., McLinden, C. A., Lu, Z., and Streets, D. G.: Disentangling the impact of the COVID-19 lockdowns on urban NO2 from natural variability, Geophysical Research Letters, 47, e2020GL089 269, 2020.

Griffin, D., Zhao, X., McLinden, C. A., Boersma, F., Bourassa, A., Dammers, E., Degenstein, D., Eskes, H., Fehr, L., Fioletov, V., et al.: High-resolution mapping of nitrogen dioxide with TROPOMI: First results and validation over the Canadian oil sands, Geophysical Research Letters, 46, 1049–1060, 2019.

Holland, F., Hofzumahaus, A., Schäfer, J., Kraus, A., and Pätz, H.-W.: Measurements of OH and HO2 radical concentrations and photolysis frequencies during BERLIOZ, Journal of Geophysical Research: Atmospheres, 108, PHO–2, 2003.

Ialongo, I., Hakkarainen, J., Hyttinen, N., Jalkanen, J.-P., Johansson, L., Boersma, K., Krotkov, N., and Tamminen, J.: Characterization of OMI tropospheric NO2 over the Baltic Sea region, Atmospheric Chemistry and Physics, 14, 7795, 2014.

Ialongo, I., Virta, H., Eskes, H., Hovila, J., and Douros, J.: Comparison of TROPOMI/Sentinel-5 Precursor NO_2 observations with ground-based measurements in Helsinki, Atmospheric Measurement Techniques, 13, 205–218, https://doi.org/10.5194/amt-13-205-2020, https://amt.copernicus.org/articles/13/205/2020/, 2020.

Inness, A., Ades, M., Agustí-Panareda, A., Barré, J., Benedictow, A., Blechschmidt, A.-M., Dominguez, J. J., Engelen, R., Eskes, H., Flemming, J., Huijnen, V., Jones, L., Kipling, Z., Massart, S., Parrington, M., Peuch, V.-H., Razinger, M., Remy, S., Schulz, M., and Suttie, M.: The CAMS reanalysis of atmospheric composition, Atmospheric Chemistry and Physics, 19, 3515–3556, https://doi.org/10.5194/acp-19-3515-2019, https://acp.copernicus.org/articles/19/3515/2019/, 2019.

Jacob, D. J.: Introduction to atmospheric chemistry, Princeton University Press, 1999.

Judd, L. M., Al-Saadi, J. A., Szykman, J. J., Valin, L. C., Janz, S. J., Kowalewski, M. G., Eskes, H. J., Veefkind, J. P., Cede, A., Mueller, M., Gebetsberger, M., Swap, R., Pierce, R. B., Nowlan, C. R., Abad, G. G., Nehrir, A., and Williams, D.: Evaluating Sentinel-5P TROPOMI tropospheric NO_2 column densities with airborne and Pandora spectrometers near New York City and Long Island Sound, Atmospheric Measurement Techniques, 13, 6113–6140, https://doi.org/10.5194/amt-13-6113-2020, https://amt.copernicus.org/articles/13/6113/2020/, 2020.

https://doi.org/10.5194/acp-2021-273
Preprint. Discussion started: 8 April 2021

Atmospheric Chemistry and Physics Discussions

Kunhikrishnan, T., Lawrence, M. G., von Kuhlmann, R., Richter, A., Ladstätter-Weißenmayer, A., and Burrows, J. P.: Analysis of tropospheric NOx over Asia using the model of atmospheric transport and chemistry (MATCH-MPIC) and GOME-satellite observations, Atmospheric Environment, 38, 581–596, 2004.

Laughner, J. L. and Cohen, R. C.: Direct observation of changing NOx lifetime in North American cities, Science, 366, 723–727, 2019.

Leue, C., Wenig, M., Wagner, T., Klimm, O., Platt, U., and Jähne, B.: Quantitative analysis of NO x emissions from Global Ozone Monitoring Experiment satellite image sequences, Journal of Geophysical Research: Atmospheres, 106, 5493–5505, 2001.

Levelt, P. F., van den Oord, G. H., Dobber, M. R., Malkki, A., Visser, H., de Vries, J., Stammes, P., Lundell, J. O., and Saari, H.: The ozone monitoring instrument, IEEE Transactions on geoscience and remote sensing, 44, 1093–1101, 2006.

Liu, F., Beirle, S., Zhang, Q., Dörner, S., He, K., and Wagner, T.: NOx lifetimes and emissions of cities and power plants in polluted background estimated by satellite observations, Atmospheric Chemistry and Physics, 16, 5283, 2016.

Liu, F., Page, A., Strode, S. A., Yoshida, Y., Choi, S., Zheng, B., Lamsal, L. N., Li, C., Krotkov, N. A., Eskes, H., et al.: Abrupt decline in tropospheric nitrogen dioxide over China after the outbreak of COVID-19, Science Advances, p. eabc2992, 2020.

Lorente, A., Boersma, K., Eskes, H., Veefkind, J., Van Geffen, J., de Zeeuw, M., van der Gon, H. D., Beirle, S., and Krol, M.: Quantification of nitrogen oxides emissions from build-up of pollution over Paris with TROPOMI, Scientific reports, 9, 1–10, 2019.

Lu, K. D., Hofzumahaus, A., Holland, F., Bohn, B., Brauers, T., Fuchs, H., Hu, M., Häseler, R., Kita, K., Kondo, Y., Li, X., Lou, S. R., Oebel, A., Shao, M., Zeng, L. M., Wahner, A., Zhu, T., Zhang, Y. H., and Rohrer, F.: Missing OH source in a suburban environment near Beijing: observed and modelled OH and HO_2 concentrations in summer 2006, Atmospheric Chemistry and Physics, 13, 1057–1080, https://doi.org/10.5194/acp-13-1057-2013, https://acp.copernicus.org/articles/13/1057/2013/, 2013.

Lu, Z., Streets, D., De Foy, B., Lamsal, L., Duncan, B., and Xing, J.: Emissions of nitrogen oxides from US urban areas: estimation from Ozone Monitoring Instrument retrievals for 2005-2014, Atmospheric Chemistry and Physics Discussions (Online), 15, 2015.

Martin, R. V., Jacob, D. J., Chance, K., Kurosu, T. P., Palmer, P. I., and Evans, M. J.: Global inventory of nitrogen oxide emissions constrained by space-based observations of NO2 columns, Journal of Geophysical Research: Atmospheres, 108, 2003.

Molina, M. J. and Molina, L. T.: Megacities and atmospheric pollution, Journal of the Air & Waste Management Association, 54, 644–680, 2004.

Munro, R., Eisinger, M., Anderson, C., Callies, J., Corpaccioli, E., Lang, R., Lefebvre, A., Livschitz, Y., and Albinana, A. P.: GOME-2 on MetOp, in: Proc. of The 2006 EUMETSAT Meteorological Satellite Conference, Helsinki, Finland, vol. 1216, p. 48, 2006.

Pommier, M., McLinden, C. A., and Deeter, M.: Relative changes in CO emissions over megacities based on observations from space, Geophysical research letters, 40, 3766–3771, 2013.

Seinfeld, J. H. and Pandis, S. N.: Atmospheric Chemistry and Physics, A Wiley-Inter Science Publication, 2006.

Seo, S., Richter, A., Blechschmidt, A.-M., Bougoudis, I., and Burrows, J. P.: First high-resolution BrO column retrievals from TROPOMI., Atmospheric Measurement Techniques, 12, 2019.

Shah, V., Jacob, D. J., Li, K., Silvern, R. F., Zhai, S., Liu, M., Lin, J., and Zhang, Q.: Effect of changing NO_x lifetime on the seasonality and long-term trends of satellite-observed tropospheric NO_2 columns over China, Atmospheric Chemistry and Physics, 20, 1483–1495, https://doi.org/10.5194/acp-20-1483-2020, https://acp.copernicus.org/articles/20/1483/2020/, 2020.

Smith, S. C., Lee, J. D., Bloss, W. J., Johnson, G. P., Ingham, T., and Heard, D. E.: Concentrations of OH and HO_2 radicals during NAMBLEX: measurements and steady state analysis, Atmospheric Chemistry and Physics, 6, 1435–1453, https://doi.org/10.5194/acp-6-1435-2006, https://acp.copernicus.org/articles/6/1435/2006/, 2006.

https://doi.org/10.5194/acp-2021-273
Preprint. Discussion started: 8 April 2021

Stavrakou, T., Müller, J.-F., Boersma, K. F., De Smedt, I., and Van Der A, R.: Assessing the distribution and growth rates of NOx emission sources by inverting a 10-year record of NO2 satellite columns, Geophysical Research Letters, 35, 2008.

Stavrakou, T., Müller, J.-F., Boersma, K. F., van der A, R. J., Kurokawa, J., Ohara, T., and Zhang, Q.: Key chemical NO_x sink uncertainties and how they influence top-down emissions of nitrogen oxides, Atmospheric Chemistry and Physics, 13, 9057–9082, https://doi.org/10.5194/acp-13-9057-2013, https://acp.copernicus.org/articles/13/9057/2013/, 2013.

Stavrakou, T., Müller, J.-F., Bauwens, M., Boersma, K., and van Geffen, J.: Satellite evidence for changes in the NO2 weekly cycle over large cities, Scientific reports, 10, 1–9, 2020.

Stocker, T.: Climate change 2013: the physical science basis: Working Group I contribution to the Fifth assessment report of the Intergovernmental Panel on Climate Change, Cambridge university press, 2014.

Valin, L., Russell, A., and Cohen, R.: Variations of OH radical in an urban plume inferred from NO2 column measurements, Geophysical Research Letters, 40, 1856–1860, 2013.

Valin, L. C., Russell, A. R., and Cohen, R. C.: Chemical feedback effects on the spatial patterns of the NO_x weekend effect: a sensitivity analysis, Atmospheric Chemistry and Physics, 14, 1–9, https://doi.org/10.5194/acp-14-1-2014, https://acp.copernicus.org/articles/14/1/2014/, 2014.

Van Der A, R., Eskes, H., Boersma, K., Van Noije, T., Van Roozendael, M., De Smedt, I., Peters, D., and Meijer, E.: Trends, seasonal variability and dominant NOx source derived from a ten year record of NO2 measured from space, Journal of Geophysical Research: Atmospheres, 113, https://doi.org/10.1029/2007JD009021, 2008.

Van Geffen, J., Eskes, H., Boersma, K., Maasakkers, J., and Veefkind, J.: TROPOMI ATBD of the total and tropospheric NO2 data products (issue 1.2. 0), Royal Netherlands Meteorological Institute (KNMI), De Bilt, the Netherlands, s5P-KNMI-L2-0005-RP, 2018.

Veefkind, J., Aben, I., McMullan, K., Förster, H., De Vries, J., Otter, G., Claas, J., Eskes, H., De Haan, J., Kleipool, Q., et al.: TROPOMI on the ESA Sentinel-5 Precursor: A GMES mission for global observations of the atmospheric composition for climate, air quality and ozone layer applications, Remote Sensing of Environment, 120, 70–83, 2012.

Verhoelst, T., Compernolle, S., Pinardi, G., Lambert, J.-C., Eskes, H. J., Eichmann, K.-U., Fjæraa, A. M., Granville, J., Niemeijer, S., Cede, A., et al.: Ground-based validation of the Copernicus Sentinel-5p TROPOMI NO 2 measurements with the NDACC ZSL-DOAS, MAX-DOAS and Pandonia global networks, Atmospheric Measurement Techniques, 14, 481–510, https://doi.org/10.5194/amt-14-481-2021, 2021.

Vrekoussis, M., Richter, A., Hilboll, A., Burrows, J., Gerasopoulos, E., Lelieveld, J., Barrie, L., Zerefos, C., and Mihalopoulos, N.: Economic crisis detected from space: Air quality observations over Athens/Greece, Geophysical Research Letters, 40, 458–463, https://doi.org/10.1002/grl.50118, 2013.